

Improved lattice Boltzmann model for immiscible multicomponent systems with high viscosity gradients at the interface

Ricardo L. M. Bazarin ^{*}

*Porous Media Research Group (PORO), Scientific Computational Laboratory,
Federal University of Santa Catarina, 89219-600 Joinville, SC, Brazil*

Christian Naaktgeboren [†]

*Hermann von Helmholtz Energy Research Group, Federal University of Technology,
Av. Guarapuava, 800. Cidade dos Lagos, 85053-525 Guarapuava, PR, Brazil*

Silvio L. M. Junqueira [‡]

*Research Center for Rheology and Non-Newtonian Fluids, Federal University of Technology, 81280-340,
R. Deputado Heitor Alencar Furtado, 5000 - Bloco N - Ecoville, Curitiba, PR, Brazil*

Paulo Cesar Philippi [§]

Mechanical Engineering Graduate Program, Pontifical Catholic University of Parana, 80215-901 Curitiba, PR, Brazil

Luiz Adolfo Hegele, Jr. [¶]

Department of Petroleum Engineering, Santa Catarina State University, 88336-275 Balneário Camboriú, SC, Brazil



(Received 30 October 2023; accepted 18 April 2024; published 8 July 2024)

We propose alternative discretization schemes for improving the lattice Boltzmann pseudopotential model for incompressible multicomponent systems, with the purpose of modeling the flow of immiscible fluids with a large viscosity ratio. Compared to the original model of Shan-Chen [*Phys. Rev. E* **47**, 1815 (1993)], the present discretization schemes consider: (i) an explicit force term, (ii) a second-order discretization of the stream term, (iii) a moments-based model for the kinetic nonequilibrium distributions, and (iv) a high-order discretization of the spatial derivative terms. To verify the accuracy of the proposed model, the effects of varying the viscosity ratio as well as both fluid's viscosities on spurious currents and capillary number are investigated for the problems dealing with a static bubble, two-component Poiseuille flow, and immiscible fluid-fluid displacement. The resulting algorithm maintains the simplicity of the pseudopotential model while allowing an easy implementation for multicomponent systems. The results of the model herein proposed show improved control of the interface region and interfacial tension, relatively smaller magnitudes of spurious current values with increasing viscosity ratio, and also a significantly wider stability range with respect to the previously best results in the literature.

DOI: [10.1103/PhysRevE.110.015303](https://doi.org/10.1103/PhysRevE.110.015303)

I. INTRODUCTION

Over the years, the lattice Boltzmann method (LBM) has become a promising alternative tool to simulate the fluid dynamics of nonideal mixtures. Originating from the evolution of the lattice-gas automaton method in the 1980s, the LBM consists of a discrete form of the Boltzmann equation that allows for a simple implementation for modeling complex systems, such as multicomponent and multiphase systems [1–3], while accounting for the underlying physics.

In the modeling of immiscible multicomponent problems, the interface of immiscible fluids is characterized by a transition layer where the molecules of each fluid are subjected to two opposite processes. Specifically, the random thermal motion of the molecules tends to mix the fluids, while the attractive intermolecular forces of each molecule from its own component tend to segregate the fluids. The prominence of attractive forces over random thermal movement leads to segregation, i.e., to an immiscible behavior, with a well-defined interface with strong density and viscosity gradients.

However, the realistic description of this fluid-fluid interface remains a major challenge for LBM's multicomponent modeling [3]. The LBM framework is not able to directly represent the random thermal movement and the molecule attractions at the microscopic scale. Lattice Boltzmann models focus on describing the mixing and segregation processes of nonideal mixtures in a mesoscopic scale based on discrete forms of kinetic equations. Therefore, modeling of

^{*}ricardo.bazarin@posgrad.ufsc.br[†]NaaktgeborenC.PhD@gmail.com[‡]silvio@utfpr.edu.br[§]paulo.philippi@pucpr.br[¶]luiz.hegele@udesc.br

immiscible multicomponent systems in LBM fundamentally relies on force models (color gradient [4,5] and pseudopotential [1,6]) and pressure models (free-energy [7,8] and interface tracking [9]). Although each of these models has its own advantages and drawbacks, all seek to simulate multicomponent systems with high viscosity and density ratio, minimal spurious currents, reduced dissolution of small bubbles, low computational cost, and other features that are requested in the simulation of complex engineering problems [10].

This work proposes an improvement of the Shan and Chen [1] pseudopotential model, focusing on stability for a large viscosity ratio at the interface. Although having simplicity and efficiency as the main characteristics, the pseudopotential model does not preserve total energy, presenting thermodynamic inconsistencies related to the failure of the model to predict a surface tension, according to the Helmholtz free energy excess theory [3]. Moreover, in the pseudopotential model: (i) the interface tension is viscosity dependent [11–13]; (ii) stability is limited to viscosity ratios up to 10; [14,15]; (iii) segregation and interface tension are governed by effects of the same order of magnitude as the errors of the discrete approximation; (iv) models are not able to simulate fluids with arbitrary equations of state; (v) models are not able to, independently control the force parameter in the equation of state and surface tension.

Previous works have been performed to improve the multicomponent pseudopotential model for immiscible fluids with a focus on representing the viscosity gradient at the interface. Porter *et al.* [16] used an explicit force term, a second-order discretization of the stream term, high-order discretization of the spatial derivative terms in the force calculation, and a multirelaxation time (MRT) collision model. Spurious currents below 10^{-3} (following the literature, all spurious currents, or velocities, are herein reported in lattice units) and a viscosity ratio of 10^3 were reported without instability issues. Otomo *et al.* [11] applied the regularization method conceptualized by Latt and Chopard [17] and Zhang *et al.* [18]. By explicitly defining the force term and using a first-order discretization of the stream term, Otomo's model achieves high viscosity ratios and spurious currents with the same orders of magnitude found by Porter *et al.* [16]. Similarly, the Gharibi and Ashrafizaadeh [19] model is based on an explicit force term, high-order discretization of the spatial derivative terms, and a modified cascaded collision model based on nonorthogonal central moments, obtaining maximum spurious currents $O(10^{-4})$ and achieving stable results for viscosity ratios until 10^4 . Considering a review of works that study large viscosity gradients with other multicomponent LBM models, Ginzburg [20] proposed a color gradient model with discontinuous collision components using an MRT collision model that achieves a viscosity ratio of the order of 10^4 . Liu *et al.* [21] work proposes a modified color-gradient model with MRT collision capable of accurately simulating viscosity ratio of order 10^4 and maximum spurious currents $O(10^{-6})$ lattice units.

In this work, an improved multicomponent model is presented to simulate immiscible fluids. The model is characterized by the integration of several discretization schemes into the original pseudopotential model. These consist of an explicit force term that eliminates the viscosity dependency of the interface tension, a second-order discretization of the

stream term, and a high-order discretization of the spatial derivatives. Furthermore, the proposal is based on a moments scheme that represents Stokes hypotheses (Stokesian model) and a smooth curve to represent the relaxation time of the mixture. A parametric analysis is conducted to investigate the numerical stability and the magnitude of spurious currents for a static bubble, two-component Poiseuille flow, and immiscible displacement problems.

The work sequence is organized as follows. In Secs. II and III, we review the standard LBM discretization and present the pseudopotential model originally proposed by Shan and Chen [1], respectively. In Sec. IV, we present the discretization schemes applied to the original model and the macroscopic equations of the modified model. The numerical simulations and the analysis of the results are presented in Sec. V. Finally, we conclude with a summary and discussion of the results in Sec. VI.

II. LATTICE BOLTZMANN METHOD FOR IMMISCIBLE MULTICOMPONENT SYSTEM

The lattice Boltzmann method for immiscible multicomponent system consists of a specific discretized form of the Boltzmann equation for nonideal mixtures of r components:

$$\frac{df^{(p)}}{dt} = \partial_t f^{(p)} + \vec{\xi} \cdot \partial_{\vec{x}} f^{(p)} + \vec{g}^e \cdot \partial_{\vec{\xi}} f^{(p)} = \sum_{s=1}^r \Omega^{(ps)},$$

$$p = 1, \dots, r. \quad (1)$$

The term \vec{g}^e is the acceleration due to external forces and $\Omega^{(ps)} = \Omega_{\text{rep}}^{(ps)} + \Omega_{\text{att}}^{(ps)}$ is the term related to the strong short-range repulsion ($\Omega_{\text{rep}}^{(ps)}$) and the weak long-range attractive forces ($\Omega_{\text{att}}^{(ps)}$) on the particle p of the particles s [22].

The short-range repulsion term is a complex integrodifferential equation that can be simplified using a collision model and further updated by adding the full Enskog's volume correction [3,23,24], which considered the molecules to be smooth rigid spheres, resulting in

$$\Omega_{\text{rep}}^{(ps)} = \Omega_{b=0}^{(ps)} + \chi^{(p)} \partial_{\vec{x}} \frac{b\rho^2 kT}{1-b\rho} \cdot \frac{\partial_{\vec{\xi}} f^{(p)}}{\rho^{(p)}}, \quad (2)$$

where T is the temperature, k is the Boltzmann constant, b is the volume of the molecule, ρ is the fluid density, $\chi^{(p)} = \rho^{(p)}/\rho$ is the p -component mass fraction and $\Omega_{b=0}^{(ps)}$ is a zero volume collision term represented by the Bhatnagar-Gross-Krook (BGK) collision model [25]. For modeling immiscible fluids there is no interest in allowing the diffusion of component p into the component s , being possible consider null the collision effect between different components, i.e., $\Omega_{b=0}^{(ps)} = 0$ for $p \neq s$ and $\Omega_{b=0}^{(ps)} = \Omega_{b=0}^{(p)}$. Replacing the collision term $\Omega_{b=0}^{(p)}$ by the BGK collision model, Eq. (2) is represented by

$$\Omega_{\text{rep}}^{(p)} = -\frac{f^{(p)} - f_{\text{eq}}^{(p)}(\rho^{(p)}, \vec{u})}{\tau} + \chi^{(p)} \partial_{\vec{x}} \frac{b\rho^2 kT}{1-b\rho} \cdot \frac{\partial_{\vec{\xi}} f^{(p)}}{\rho^{(p)}}, \quad (3)$$

where f_{eq} is the equilibrium distribution function and τ is the relaxation time given as a function of the thermodynamic properties of all components, i.e., $\tau(\rho^{(p)}, \rho^{(s)}, \dots, \rho^{(r)}, \theta^{(p)}, \theta^{(s)}, \dots, \theta^{(r)})$.

Similar to the short-range term, the long-range attractive term is represented by another integral responsible for representing the nonideal behavior of the r components system. In order to simplify this complex equation the mean-field approximation is applied resulting in a force term representation in the form

$$\begin{aligned}\Omega_{\text{att}}^{(ps)} &= \vec{g}^{(ps)} \cdot \partial_{\vec{x}} f^{(p)} \\ &= (-2a^{(ps)} \partial_{\vec{x}} \rho^{(p)} + \kappa^{(ps)} \partial_{\vec{x}} \partial_{\vec{x}}^2 \rho^{(p)}) \cdot \partial_{\vec{x}} f^{(p)},\end{aligned}\quad (4)$$

where $\vec{g}^{(ps)}$ is the intermolecular long-range acceleration, $a^{(ps)}$ and $\kappa^{(ps)}$ are parameters dependent on the $p-s$ intermolecular interaction [3].

The discretized form in the velocity space of Eq. (1) with Eqs. (4) and (3), is represented in the form

$$\begin{aligned}\partial_t f_i^{(p)} + \vec{e}_i \cdot \partial_{\vec{x}} f_i^{(p)} &= -\frac{f_i^{(p)} - f_{\text{eq},i}^{(p)}(\rho^{(p)}, \vec{u})}{\tau} \\ &+ \left(\rho^{(p)} \vec{g}^e - \chi^{(p)} \partial_{\vec{x}} \frac{b\rho^2 c_s^2}{1-b\rho} + \sum_{s=1}^r \rho^{(p)} \vec{g}^{(ps)} \right) \cdot \frac{\partial_{\vec{e}_i} f_i^{(p)}}{\rho^{(p)}},\end{aligned}\quad (5)$$

where \vec{e}_i , $i = 0, \dots, b$, represents the set of dimensionless lattice vectors and τ is determined by

$$\tau = \frac{\nu}{c_s^2},\quad (6)$$

where ν is the kinematic viscosity of the mixture of components and c_s is the speed of sound.

The equilibrium distribution function is given by the Maxwell-Boltzmann equilibrium distribution. Using a second-order approximation, the equilibrium distribution function is written in its discretized form as [26]

$$f_{\text{eq},i}^{(p)}(\rho^{(p)}, \vec{u}) = \rho^{(p)} w_i \left(1 + \frac{\vec{e}_i \cdot \vec{u}}{c_s^2} + \frac{1}{2c_s^4} \vec{u} \vec{u} : (\vec{e}_i \vec{e}_i - c_s^2 I) \right),\quad (7)$$

where ρ is the density, \vec{u} is the velocity vector and w_i are the weight factors. The macroscopic properties are recovered from the moments of the distribution functions, i.e.,

$$\rho = \sum_p \rho^{(p)} = \sum_p \sum_i f_i^{(p)},\quad (8)$$

$$\rho \vec{u} = \sum_p \rho^{(p)} \vec{u}^{(p)} = \sum_p \sum_i \vec{e}_i f_i^{(p)}.\quad (9)$$

In the discretization of the velocity space, a second-order approximation for nine points was used, obtaining the two-dimensional set of lattice vectors D2Q9, where

$$\vec{e}_{i=0} = (0, 0),$$

$$\vec{e}_{i=1,2,3,4} = \left(\cos \frac{i-1}{2} \pi, \sin \frac{i-1}{2} \pi \right),$$

$$\vec{e}_{i=5,6,7,8} = \sqrt{2} \left(\cos \frac{i-5}{2} \pi + \frac{\pi}{4}, \sin \frac{i-5}{2} \pi + \frac{\pi}{4} \right).\quad (10)$$

The D2Q9 lattice weight factors are given by $w_0 = 4/9$, $w_i = 1/9$ for $i = 1, 2, 3, 4$; and $w_i = 1/36$ for $i = 5, 6, 7, 8$; and the sound speed by $c_s = 1/\sqrt{3}$.

Applying the Chapman-Enskog analysis in Eq. (5) and integration over moments, the macroscopic equations are recovered:

$$\partial_t \rho^{(p)} + \partial_{\vec{x}} \cdot (\rho^{(p)} \vec{u}) = 0,\quad (11)$$

$$\partial_t \rho + \partial_{\vec{x}} \cdot (\rho \vec{u}) = 0,\quad (12)$$

$$\partial_t (\rho \vec{u}) + \partial_{\vec{x}} \cdot (\rho \vec{u} \vec{u} + \mathbf{P} - \rho \nu (\partial_{\vec{x}} \vec{u} + (\partial_{\vec{x}} \vec{u})^T)) = \rho \vec{g}^e,\quad (13)$$

where Eq. (11) represents the mass balance for the component p , Eq. (12) represents the mass balance of the mixture and Eq. (13) the momentum balance for the mixture, \mathbf{P} being the pressure tensor represented by

$$\mathbf{P} = P_s \mathbf{I} + \mathbf{S},\quad (14)$$

the scalar pressure is given by

$$\begin{aligned}P_s &= P_e - \frac{1}{2} \left(\partial_{\vec{x}}^2 (\kappa \rho^2) - \sum_{p,s} \kappa^{(ps)} \partial_{\vec{x}} \rho^{(p)} \cdot \partial_{\vec{x}} \rho^{(s)} \right), \\ \kappa &= \sum_{p,s} \chi^{(p)} \chi^{(s)} \kappa^{(ps)},\end{aligned}\quad (15)$$

the thermodynamic pressure by

$$P_e = \frac{\rho c_s^2}{1-b\rho} - a \rho^2, \quad a = \sum_{p,s} \chi^{(p)} \chi^{(s)} a^{(ps)},\quad (16)$$

and the interface Korteweg tensor by

$$\mathbf{S} = \sum_{p,s} \kappa^{(ps)} (\partial_{\vec{x}} \rho^{(p)} \partial_{\vec{x}} \rho^{(s)}).\quad (17)$$

III. MULTICOMPONENT PSEUDOPOTENTIAL MODEL

The pseudopotential model was conceived to represent nonideal mixtures based on potential mass forces between the particles of each component [1]. The pseudo-potential lattice Boltzmann (LB) equation for r components is described by

$$f_i^{(p)}(\vec{x} + \vec{e}_i \delta_t, t + \delta_t) = f_i^{(p)}(\vec{x}, t) + \frac{f_{\text{eq},i}^{(p)}(\rho_{\sigma}, \vec{u}_*^{(p)}) - f_i^{(p)}}{\tau^{(p)}},\quad (18)$$

where δ_t is time increment coupled to the lattice vectors, being defined as a unit value (i.e., $\delta_t = 1$). The shifted velocity $\vec{u}_*^{(p)}$ in the equilibrium distribution function is given by

$$\vec{u}_*^{(p)} = \frac{\sum_s \frac{\rho^{(s)} \vec{u}^{(s)}}{\tau^{(s)}}}{\sum_s \frac{\rho^{(s)}}{\tau^{(s)}}} + \tau^{(p)} \vec{g}^{(p)},\quad (19)$$

where $\rho^{(p)}$ and $\rho^{(p)} \vec{u}^{(p)}$ are recovered from Eqs. (8) and (9), respectively.

By representing the pseudopotential LB equation in the explicit form of the force term

$$f_i^{(p)'} = f_i^{(p)} + \frac{f_{\text{eq},i}^{(p)}(\rho_\sigma, \vec{u}') - f_i^{(p)}}{\tau^{(p)}} + \delta_t F_i^{(p)}, \quad (20)$$

where $f_i^{(p)'} = f_i^{(p)}(\vec{x} + \vec{e}_i \delta_t, t + \delta_t)$, the term $F_i^{(p)}$ is represented by

$$F_i^{(p)} = w_i \rho^{(p)} \left(\frac{\vec{e}_i \cdot \vec{g}^{(p)}}{c_s^2} + \frac{(\vec{e}_i \vec{e}_i - c_s^2 \mathbf{I})}{2c_s^4} : \Lambda_{SC}^{(p)} \right), \quad (21)$$

where $\Lambda_{SC}^{(p)} = (\vec{g}^{(p)} \vec{u}' + (\vec{g}^{(p)} \vec{u}')^T + \tau^{(p)} \vec{g}^{(p)} \vec{g}^{(p)})$ and \vec{u}' is given by

$$\vec{u}' = \frac{\sum_s \frac{\rho^{(s)} \vec{u}^{(s)}}{\tau^{(s)}}}{\sum_s \frac{\rho^{(s)}}{\tau^{(s)}}}. \quad (22)$$

The acceleration $\vec{g}^{(p)}$ produced by the intermolecular forces between component p and the mixture components \bar{p} is formulated as

$$\vec{g}^{(p)} = \vec{g}^e + \frac{\Psi^{(p)}}{\rho^{(p)}} \sum_{\bar{p}} G^{(p\bar{p})} \sum_i w_i(\vec{e}_i) \Psi^{(\bar{p})}(\vec{x} + \vec{e}_i, t) \vec{e}_i \quad (23)$$

where Ψ is a virtual mass, \bar{p} indicates a mixture component different from p and $G^{(p\bar{p})}$ referred as the interaction strength, is a molecular parameter only dependent on the $p - \bar{p}$ intermolecular interaction. Conceived as a repulsion potential, the parameter $G^{(p\bar{p})}$ is responsible for the segregation process at the interface. Expanding Eq. (23) in Taylor series to represent the virtual mass $\Psi^{(p)}(\vec{x} + \vec{e}_i, t)$ in terms of $\Psi^{(p)}(\vec{x}, t)$ (Einstein

notation will be used in this development), we have

$$(g_\alpha^{(p)} - g_\alpha^e) = \frac{\Psi^{(p)}}{\rho^{(p)}} \sum_{\bar{p}} G^{(p\bar{p})} \left(E^{(1)} \Psi^{(\bar{p})} + E^{(2)} \partial_\alpha \Psi^{(\bar{p})} + \frac{1}{2} E^{(3)} \partial_{\alpha\beta} \Psi^{(\bar{p})} + \frac{1}{6} E^{(4)} \partial_{\alpha\beta\gamma} \Psi^{(\bar{p})} + \dots \right), \quad (24)$$

where $E^{(n)}$ are tensors of order n represented by

$$E^{(n)} = E_{\alpha_1, \alpha_2, \dots, \alpha_n}^{(n)} = \sum_i^d w_i e_{i, \alpha_1} e_{i, \alpha_2} \dots e_{i, \alpha_n}. \quad (25)$$

Taking the isotropy of the discrete velocity-space into account, odd-order tensors are null ($E^{(2n-1)} = 0$), and even-order tensors are given by

$$E^{(2n)} = c_s^{2n} \delta_{\alpha_1, \alpha_2, \dots, \alpha_n}^{(2n)}, \quad (26)$$

where $\delta_{\alpha_1, \alpha_2, \dots, \alpha_n}^{(2n)}$ is the generalized Kronecker delta of order $2n$ and means the sum of all possible combinations of Kronecker delta products, i.e, for $E^{(4)}$ as an example $E^{(4)} = c_s^4 (\delta_{\alpha\beta} \delta_{\gamma\delta} + \delta_{\alpha\gamma} \delta_{\beta\delta} + \delta_{\alpha\delta} \delta_{\beta\gamma})$. Truncating the Eq. (52) in fifth-order terms and substituting the tensors are recovered the pseudopotential mean-field approximation

$$(g_\alpha^{(p)} - g_\alpha^e) = \frac{\Psi^{(p)}}{\rho^{(p)}} \sum_{\bar{p}} G^{(p\bar{p})} \left(c_s^2 \partial_\alpha \Psi^{(\bar{p})} + \frac{c_s^4}{2} \partial_{\alpha\beta\beta} \Psi^{(\bar{p})} \right). \quad (27)$$

A. Macroscopic balance equations

Applying a Chapman-Enskog analysis to the Eq. (20), the balance equations of mass and momentum balance are recovered for the components and mixture:

$$\partial_t \rho^{(p)} + \partial_{\vec{x}} \cdot (\rho^{(p)} \vec{u}') + \left(1 - \frac{1}{2\tau^{(p)}} \right) \partial_{\vec{x}} \cdot \vec{m}_{(1)}^{(p)} = -\frac{1}{2} \partial_{\vec{x}} \cdot (\rho^{(p)} \vec{g}^{(p)}), \quad (28)$$

$$\partial_t \rho + \partial_{\vec{x}} \cdot (\rho \vec{u}') = -\sum_p \left(\partial_{\vec{x}} \cdot \vec{m}_{(1)}^{(p)} \right) - \frac{1}{2} \partial_{\vec{x}} \cdot (\rho^{(p)} \vec{g}^{(p)}), \quad (29)$$

$$\begin{aligned} \partial_t (\rho^{(p)} \vec{u}') + \partial_{\vec{x}} \cdot (\rho^{(p)} \vec{u}' \vec{u}') + \frac{\rho^{(p)}}{\rho} \partial_{\vec{x}} \cdot \mathbf{P}_{SC} - \rho^{(p)} \vec{g}^e + \left(1 - \frac{1}{2\tau^{(p)}} \right) \left(\partial_t \vec{m}_{(1)}^{(p)} + \partial_{\vec{x}} \cdot \left(\vec{m}_{(1)}^{(p)} \vec{u}' + (\vec{m}_{(1)}^{(p)} \vec{u}')^{(T)} \right) \right) \\ - \left(\tau^{(p)} - \frac{1}{2} \right) \left(\partial_{\vec{x}} \cdot \rho^{(p)} (\partial_{\vec{x}} \vec{u}' + (\partial_{\vec{x}} \vec{u}')^T) \right) = -\frac{1}{2} \partial_t (\rho^{(p)} \vec{g}^{(p)}) - \frac{1}{2} \partial_{\vec{x}} \cdot (\rho^{(p)} (\vec{g}^{(p)} \vec{u}' + (\vec{g}^{(p)} \vec{u}')^T + \tau^{(p)} \vec{g}^{(p)} \vec{g}^{(p)})), \end{aligned} \quad (30)$$

$$\begin{aligned} \partial_t (\rho \vec{u}') + \partial_{\vec{x}} \cdot (\rho \vec{u}' \vec{u}') + \partial_{\vec{x}} \cdot \mathbf{P}_{SC} - \sum_p \left(\left(\tau^{(p)} - \frac{1}{2} \right) \left(\partial_{\vec{x}} \cdot \rho^{(p)} (\partial_{\vec{x}} \vec{u}' + (\partial_{\vec{x}} \vec{u}')^T) \right) \right) - \rho \vec{g}^e \\ = -\sum_p \partial_t \vec{m}_{(1)}^{(p)} + \partial_{\vec{x}} \cdot \sum_p \left(\vec{m}_{(1)}^{(p)} \vec{u}' - (\vec{m}_{(1)}^{(p)} \vec{u}')^{(T)} \right) - \frac{1}{2} \sum_p \left(\partial_t (\rho^{(p)} \vec{g}^{(p)}) + \partial_{\vec{x}} \cdot (\rho^{(p)} (\vec{g}^{(p)} \vec{u}' + (\vec{g}^{(p)} \vec{u}')^T + \tau^{(p)} \vec{g}^{(p)} \vec{g}^{(p)})) \right), \end{aligned} \quad (31)$$

where $\rho v = \sum_p (\tau^{(p)} - \frac{1}{2}) c_s^2 \rho^{(p)}$, v is kinematic viscosity, and \mathbf{P}_{sc} is the pressure tensor of pseudopotential represented by

$$\mathbf{P}_{sc} = \sum_p \left(\rho^{(p)} c_s^2 \mathbf{I} - (\vec{g}^{(p)} - \vec{g}^e) \right) = P_s \mathbf{I} + \mathbf{S}, \quad (32)$$

where the scalar pressure is

$$P_s = P_e - \frac{1}{4} \sum_{p, \bar{p}} c_s^4 G^{(p\bar{p})} \left(\partial_{\vec{x}}^2 (\Psi^{(p)} \Psi^{(\bar{p})}) - \partial_{\vec{x}} \Psi^{(p)} \cdot \partial_{\vec{x}} \Psi^{(\bar{p})} \right), \quad (33)$$

the thermodynamic pressure is

$$P_e = \rho c_s^2 - \frac{1}{2} \sum_{p, \bar{p}} c_s^2 G^{(p\bar{p})} \Psi^{(p)} \Psi^{(\bar{p})}, \quad (34)$$

and the interface tension or Korteweg tensor is

$$\mathbf{S} = \sum_{p, \bar{p}} \frac{1}{2} c_s^4 G^{(p\bar{p})} (\partial_{\bar{x}} \Psi^{(p)} \partial_{\bar{x}} \Psi^{(\bar{p})}), \quad (35)$$

being $a^{(p\bar{p})}$ and $\kappa^{(p\bar{p})}$ a function of $G^{(p\bar{p})}$ (i.e., $a^{(p\bar{p})} = c_s^2 G^{(p\bar{p})}$ and $\kappa^{(p\bar{p})} = \frac{1}{2} c_s^4 G^{(p\bar{p})}$). The first-order non-equilibrium term $\bar{m}_{(1)}^{(p)}$ is given by

$$\bar{m}_{(1)}^{(p)} = \tau^{(p)} \left(\frac{\rho^{(p)}}{\rho} \partial_{\bar{x}} \cdot \mathbf{P}_{SC} - \partial_{\bar{x}} (\rho^{(p)} c_s^2) + \rho^{(p)} (\bar{g}^{(p)} - \bar{g}^e) \right). \quad (36)$$

For details of Chapman-Enskog analysis see Appendix.

The Eq. (28) represents the mass balance of the component and $\bar{m}_{(1)}^{(p)}$ is interpreted as the diffusion terms in the multi-component mixture. On the right-hand side of Eq. (28), the acceleration term is a numerical error due to the use of first-order space-time discretization. Summing the Eq. (28) over all components, Eq. (29) represents the balance mass of the mixture with discretization errors on the right-hand side. The term $\bar{m}_{(1)}^{(p)}$ when summed by all components does not become null and the acceleration term is carried from Eq. (28), but both do not affect the conservation of global mass due to your isotropic behaviors.

On Eq. (30), the momentum balance is recovered with discretization errors resulting from the space-time's first-order discretization and shifted velocity consideration. For the momentum balance of the mixture (Eq. 30) the errors (30) are maintained and the errors of $\bar{m}_{(1)}^{(p)}$ are added.

Both the mass and momentum balance equations are functions of the vector velocity \vec{u}' and of $\bar{m}_{(1)}^{(p)}$, which are dependent $\tau^{(p)}$ that vary according to the viscosity ratio of the problem. Assuming $\tau^{(p)} = \tau^{(\bar{p})}$ (i.e., $M_v = 1$) the errors of $\bar{m}_{(1)}^{(p)}$ on the right-hand side of Eqs. (29) and (31) become null and $\vec{u}' = \vec{u}$. Consequently, both terms can be sources of errors that limit stability for high-viscosity ratios.

B. Modeling comparison

The pseudopotential model can be seen as a simplified form of the model kinetic model described by Eq. (5), since in the pseudopotential model:

- (1) the volume correction of Enskog is not taken into account, i.e., $b = 0$;
- (2) the long-range forces $\bar{g}^{(ps)}$ are represented by Eq. (23) disregarding the interactions when $p = s$;
- (3) parameters $a^{(p\bar{p})}$ and $\kappa^{(p\bar{p})}$ are a function of $G^{(p\bar{p})}$;
- (4) the force terms are shifted to the collision term, resulting in the force model proposed by Shan and Chen [1];
- (5) the collision term is modified for a function of each component relaxation time ($\tau^{(p)}$).

However, the main difference between the models remains in the representation of the interactions between particles as repulsive by Eq. (23), while the forces are considered attractive by the mean-field approximations in Eq. (5).

IV. IMPROVED PSEUDOPOTENTIAL MODEL

An improved pseudopotential model is formulated in order to extend the original formulation represented by Eq. (18) for more representative modeling of the immiscible multicomponent system, as described by Eq. (5). These improvements are based on the adjustments of discretization and in the use of a moments-based collision model, both to reduce numerical errors of modeling and discretization observed in the Sec. III A.

A. Relaxation time

The relaxation time τ present in the BGK collision model is a parameter related to the mean free path and the mean velocity of the molecules representing the fluids. In the multicomponent system of r components, the relaxation time can vary according to the number of molecules of each component interacting in that position, i.e., $\tau^{p,s,\dots,r}(\vec{x}, t)$ is a function of the components, position and time. On the mesoscopic scale, the relaxation time can be approximated as a function of thermodynamic properties such as the density and temperature of fluids, it being possible to write $\tau(\vec{x}, t, \rho, \xi^{(p)}, \xi^{(s)}, \dots, \xi^{(r)}, \theta, \theta^{(p)}, \theta^{(s)}, \dots, \theta^{(r)})$, where $\theta^{(p)}$ is the mass fraction of the component p . Considering an isothermal system, the present work proposes a smooth function to represent relaxation time given by

$$\tau = \sum_p \left(\tau^{(p)} (\chi^{(p)})^{\frac{\sum_{\bar{p}} \rho^{(\bar{p})}}{\rho^{(p)}}} \right), \quad (37)$$

where the values of $\tau^{(p)}$ are determined by the relation with the kinematic viscosity obtained from the Chapman-Enskog analysis. Equation (37) creates a high viscosity gradient at the fluid-fluid interface, wherein regions characterized by a higher component density p tend to approximate the viscosity as $\tau \approx \tau^{(p)}$ avoiding density dependence.

The smoothed equation $\tau = \sum_p \chi^{(p)} \tau^{(p)}$, as employed by Otomo *et al.* [11] and Zhao *et al.* [27], exhibits a pronounced dependence on the mixture density. In this context, the local fluid density constrains the representation of high viscosity ratios.

B. Explicit force term

The force scheme initially proposed for the pseudopotential model is represented by the velocity $\vec{u}_*^{(p)}$ that incorporates the force per unit of mass $\bar{g}^{(p)}$ in the equilibrium distribution function. According to Yu *et al.* [28], Huang *et al.* [12], Li *et al.* [29], Porter *et al.* [16], and Peng *et al.* [13], this scheme has shown thermodynamic inconsistencies such as the dependence of the surface tension on the relaxation time τ . As demonstrated by Huang *et al.* [12], the velocity-shifted model results in the extra $\tau^{(p)} \bar{g}^{(p)} \bar{g}^{(p)}$ term compared to the model of Luo [30], which is based on a simplification of the distribution function to the equilibrium distribution function, i.e.,

$$\bar{g}^{(p)} \cdot \partial_{\vec{e}_i} f_i^{(p)} \approx \bar{g}^{(p)} \cdot \partial_{\vec{e}_i} f_{\text{eq},i}^{(p)}. \quad (38)$$

Employing an expansion in Hermite polynomials to write the force term simplified by an equilibrium distribution function, Shan *et al.* [31] proposed a correction for the force term with shifted velocity that eliminates the extra term. Therefore, the present work uses for the representation of the force term an

expansion to the second order of the Hermite polynomials in the equilibrium distribution function, resulting in

$$F_i^{(p)} = w_i \rho^{(p)} \left(\frac{\vec{e}_i \cdot \vec{g}^{(p)}}{c_s^2} + \frac{(\vec{e}_i \vec{e}_i - c_s^2 \mathbf{I})}{2c_s^4} : \Lambda^{(p)} \right), \quad (39)$$

where $\Lambda^{(p)} = \vec{g}^{(p)} \vec{u} + (\vec{g}^{(p)} \vec{u})^T$. The force described by Eq. (39) is equivalent to the force term presented by Luo [30]. With the extension to a second-order discretization of the streaming term, this representation of the force term recovers the scheme obtained by Guo *et al.* [32] in the lattice Boltzmann equation (Eq. 43).

C. Second-order discretization of the streaming term

He *et al.* [33] investigated a second-order discretization of the stream term when the kinetic equation includes a force term. LB schemes based on first-order discretization of the stream term are only successful because the second-order errors contribute as a numerical viscosity which is absorbed into the momentum balance equation. This is not the case when the kinetic equation includes an intermolecular force as is the case for multicomponent systems.

The lattice Boltzmann equation of the pseudopotential model [Eq. (18)] represented by a first-order discretization of the streaming term is extended for the second-order. In the discretization of the Eq. (1), the streaming term (space-time) is initially represented by an expansion in Taylor series of the forward term to a first-order forward difference of the $D_t f_i^{(p)} = \partial_t f_i^{(p)} + \vec{\xi} \cdot \partial_{\vec{x}} f_i^{(p)}$ term, algebraically written in the simplified form by

$$\begin{aligned} f_i^{(p)}(\vec{x} + \vec{e}_i \delta_t, t + \delta_t) &= f_i^{(p)}(\vec{x}, t) + \delta D_t f_i^{(p)} \\ &+ \frac{\delta^2}{2} D_t^2 f_i^{(p)} + \dots \\ &= f_i^{(p)}(\vec{x}, t) + \sum_{j=1}^{\infty} \frac{\delta^j}{j!} D_t^j f_i^{(p)}. \end{aligned} \quad (40)$$

From this point, the truncation order on the right-hand side of Eq. (40) represents the discretization order of the time-space. For a second-order truncation,

Eq. (40) reduces to

$$\begin{aligned} f_i^{(p)}(\vec{x} + \vec{e}_i \delta_t, t + \delta_t) &= f_i^{(p)}(\vec{x}, t) + \delta D_t f_i^{(p)} \\ &+ \frac{\delta^2}{2} D_t^2 f_i^{(p)} + \mathcal{O}(\delta^3), \end{aligned} \quad (41)$$

replacing the derivative term of $D_t f_i^{(p)} = \Omega_i^{(p)} + F_i^{(p)}$ and applying the first-order forward difference in the term $D_t \Omega_i^{(p)}$, we have

$$\begin{aligned} f_i^{(p)}(\vec{x} + \vec{e}_i \delta_t, t + \delta_t) &= f_i^{(p)}(\vec{x}, t) + \frac{\delta}{2} [\Omega_i^{(p)}(\vec{x} + \vec{e}_i \delta_t, t + \delta_t) + \Omega_i^{(p)}(\vec{x}, t)] \\ &+ \frac{\delta}{2} [F_i^{(p)}(\vec{x} + \vec{e}_i \delta_t, t + \delta_t) + F_i^{(p)}(\vec{x}, t)]. \end{aligned} \quad (42)$$

Since $f_i^{(p)}(\vec{x} + \vec{e}_i \delta_t, t + \delta_t)$ is an unknown value and depends on $\Omega_i^{(p)}(\vec{x} + \vec{e}_i \delta_t, t + \delta_t)$ which is another unknown value in time t . In this way, the implicit numerical scheme is achieved considering $\hat{f}_i^{(p)} = f_i^{(p)} - \frac{\delta_t}{2} (\Omega_i^{(p)} + F_i^{(p)})$, obtaining the final form of LB equation in the second-order:

$$\hat{f}_i^{(p)'} = \hat{f}_i^{(p)} + \frac{f_{\text{eq},i}^{(p)} - \hat{f}_i^{(p)}}{\hat{\tau}} + \left(1 - \frac{1}{2\hat{\tau}}\right) F_i^{(p)} \delta_t, \quad (43)$$

where $\hat{\tau} = \frac{\tau}{\delta_t} + \frac{1}{2}$.

Using the implicit scheme that redefines the distribution function in the LBE, the macroscopic properties are rewritten as a function of $\hat{f}_i^{(p)}$ by

$$\rho = \sum_p \rho^{(p)} = \sum_p \sum_i \hat{f}_i^{(p)}, \quad (44)$$

$$\rho \vec{u} = \sum_p \rho^{(p)} \vec{u}^{(p)} = \sum_p \left(\sum_i \vec{e}_i \hat{f}_i^{(p)} + \frac{\delta_t}{2} \vec{g}^{(p)} \rho^{(p)} \right). \quad (45)$$

D. Moments-based scheme

We follow the work of Asinari [34] on MRT models for homogeneous mixtures, based on the expansion of the collision operator in Hermite polynomials and taking into account the shear and bulk viscosities and species diffusion. The collision repulsion term is then represented by the relaxation of nonequilibrium moments, Eq. (43) being now described by

$$\hat{f}_i^{(p)'} = \hat{f}_i^{(p)} + M^{-1} S M \left[f_{\text{eq},i}^{(p)} + \hat{f}_i^{(p)} + \frac{F_i^{(p)} \delta_t}{2} \right] + F_i^{(p)} \delta_t, \quad (46)$$

where M is the matrix of moments based on Hermite polynomials, given by

$$M = \begin{bmatrix} 1 & 1 & 1 & 1 & 1 & 1 & 1 & 1 & 1 \\ 0 & 1 & 0 & -1 & 0 & 1 & -1 & -1 & 1 \\ 0 & 0 & 1 & 0 & -1 & 1 & 1 & -1 & -1 \\ -\frac{1}{3} & \frac{2}{3} & -\frac{1}{3} & \frac{2}{3} & -\frac{1}{3} & \frac{2}{3} & \frac{2}{3} & \frac{2}{3} & \frac{2}{3} \\ -\frac{1}{3} & -\frac{1}{3} & \frac{2}{3} & -\frac{1}{3} & \frac{2}{3} & \frac{2}{3} & \frac{2}{3} & \frac{2}{3} & \frac{2}{3} \\ 0 & 0 & 0 & 0 & 0 & 1 & -1 & 1 & -1 \\ 0 & -\frac{1}{3} & 0 & \frac{1}{3} & 0 & \frac{2}{3} & -\frac{2}{3} & -\frac{2}{3} & \frac{2}{3} \\ 0 & 0 & -\frac{1}{3} & 0 & \frac{1}{3} & \frac{2}{3} & \frac{2}{3} & -\frac{2}{3} & -\frac{2}{3} \\ \frac{1}{9} & -\frac{2}{9} & -\frac{2}{9} & -\frac{2}{9} & -\frac{2}{9} & \frac{4}{9} & \frac{4}{9} & \frac{4}{9} & \frac{4}{9} \end{bmatrix}, \quad (47)$$

for the D2Q9. The relaxation matrix S should have the form

$$S = \begin{bmatrix} 0 & 0 & 0 & 0 & 0 & 0 & 0 & 0 & 0 \\ 0 & \frac{1}{\hat{\tau}_1} & 0 & 0 & 0 & 0 & 0 & 0 & 0 \\ 0 & 0 & \frac{1}{\hat{\tau}_2} & 0 & 0 & 0 & 0 & 0 & 0 \\ 0 & 0 & 0 & \frac{1}{2\hat{\tau}_3} + \frac{1}{2\hat{\tau}_4} & \frac{1}{2\hat{\tau}_3} - \frac{1}{2\hat{\tau}_4} & 0 & 0 & 0 & 0 \\ 0 & 0 & 0 & \frac{1}{2\hat{\tau}_3} - \frac{1}{2\hat{\tau}_4} & \frac{1}{2\hat{\tau}_3} + \frac{1}{2\hat{\tau}_4} & 0 & 0 & 0 & 0 \\ 0 & 0 & 0 & 0 & 0 & \frac{1}{\hat{\tau}_5} & 0 & 0 & 0 \\ 0 & 0 & 0 & 0 & 0 & 0 & 1 & 0 & 0 \\ 0 & 0 & 0 & 0 & 0 & 0 & 0 & 1 & 0 \\ 0 & 0 & 0 & 0 & 0 & 0 & 0 & 0 & 1 \end{bmatrix}, \quad (48)$$

to correctly recover the species-diffusion and Navier-Stokes equations (Asinari [34]).

In the present work the relaxation times $\hat{\tau}_1$ and $\hat{\tau}_2$ related to the diffusion processes [described in pseudopotential models by the term (36)] are made equal to 1 seeking to minimize diffusion, $\tau_3 = 1$, relax the symmetric part of the viscous stress tensor to equilibrium and $\hat{\tau}_4 = \hat{\tau}_5 = \hat{\tau}$ are related to kinematic viscosity.

Rewriting the Eq. (46) in a way suitable for efficient numerical implementation, we have the moments-based LB scheme in the form

$$\hat{f}_i^{(p)'} = f_{\text{eq},i}^{(p)} + \left(1 - \frac{1}{\hat{\tau}}\right) \hat{f}_{\text{neq},i}^{(p)} + \left(1 - \frac{1}{2\hat{\tau}}\right) F_i^{(p)} \delta, \quad (49)$$

where

$$\hat{f}_{\text{neq},i}^{(p)} = w_i \left(\frac{(\vec{e}_i \vec{e}_i - c_s^2 \mathbf{I})}{2c_s^4} : \hat{\Pi}_{\text{neq}}^{(p)} \right) - \frac{\delta_i}{2} F_i^{(p)}, \quad (50)$$

where $\hat{\Pi}_{\text{neq}}^{(p)}$ is a corrected second-order tensor obtained by

$$\hat{\Pi}_{\text{neq}}^{(p)} = \sum_i \left(\hat{f}_i^{(p)} - f_{i,\text{eq}}^{(p)} + \frac{\delta_i}{2} F_i^{(p)} \right) \left(\vec{e}_i \vec{e}_i - \frac{\vec{e}_i \cdot \vec{e}_i \mathbf{I}}{d} \right), \quad (51)$$

where d is the lattice dimension.

E. Force model

In Eq. (23), a Taylor series expansion is used for representing the pseudopotential $\Psi^{(p)}(\vec{x} + \vec{e}_i h, t)$ in terms of $\Psi^{(p)}(\vec{x}, t)$. In this subsection Einstein's notation will be employed. The expanded result is

$$\begin{aligned} (g_\alpha^{(p)} - g_\alpha^e) &= \frac{\Psi^{(p)}}{\rho^{(p)}} \sum_{\bar{p}} G^{(p\bar{p})} \left(E^{(1)} \Psi^{(\bar{p})} + E^{(2)} \partial_\alpha \Psi^{(\bar{p})} \right. \\ &\quad \left. + \frac{1}{2} E^{(3)} \partial_{\alpha\beta} \Psi^{(\bar{p})} + \frac{1}{6} E^{(4)} \partial_{\alpha\beta\gamma} \Psi^{(\bar{p})} + \dots \right), \end{aligned} \quad (52)$$

where $E^{(n)}$ are tensors of order n represented by

$$E^{(n)} = E_{\alpha_1, \alpha_2, \dots, \alpha_n}^{(n)} = \sum_i w_i \vec{e}_{i, \alpha_1} \vec{e}_{i, \alpha_2} \dots \vec{e}_{i, \alpha_n}. \quad (53)$$

Taking the isotropy of the discrete velocity space into account, odd-order tensors are null ($E^{(2n-1)} = 0$) and even-order

tensors are given by

$$E^{(2n)} = c_s^{2n} \delta_{\alpha_1, \alpha_2, \dots, \alpha_n}^{(2n)}, \quad (54)$$

where $\delta_{\alpha_1, \alpha_2, \dots, \alpha_n}^{(2n)}$ is the generalized Kronecker delta of order $2n$ and it means the sum of all possible combinations of Kronecker delta products, i.e., for $E^{(4)}$ as an example $E^{(4)} = c_s^4 (\delta_{\alpha\beta} \delta_{\gamma\delta} + \delta_{\alpha\gamma} \delta_{\beta\delta} + \delta_{\alpha\delta} \delta_{\beta\gamma})$. Truncating the Eq. (52) in fifth-order terms and replacing tensors, we have

$$(g_\alpha^{(p)} - g_\alpha^e) = \frac{\Psi^{(p)}}{\rho^{(p)}} \sum_{\bar{p}} G^{(p\bar{p})} \left(c_s^2 \partial_\alpha \Psi^{(\bar{p})} + \frac{c_s^4}{2} \partial_{\alpha\beta\beta} \Psi^{(\bar{p})} \right). \quad (55)$$

Simplified and filtered the derivative terms of order greater than the fourth order, the Eq. (55) consists of a similar form of the Eq. (4) disregarding the interaction between when $p = s$. To better represent Eq. (4) the $G^{(p\bar{p})}$ coefficient is divided into two terms, with the term $a^{(p\bar{p})}$ controlling the separation of components and $\kappa^{(p\bar{p})}$ the surface tension between them. Consequently, Eq. (55) is rewritten in the form

$$(g_\alpha^{(p)} - g_\alpha^e) = \frac{\Psi^{(p)}}{\rho^{(p)}} \sum_{\bar{p}} \left(a^{(p\bar{p})} \partial_\alpha \Psi^{(\bar{p})} + \kappa^{(p\bar{p})} \partial_{\alpha\beta\beta} \Psi^{(\bar{p})} \right). \quad (56)$$

F. High-order discretization of the spatial derivatives

Discretizing the derivative terms present in the force model, we use the lattice stencil scheme presented by Mattila *et al.* [35]:

$$\partial_{\vec{x}} \Psi^{(\bar{p})} = \frac{1}{2c_s^2} \sum_i w_i \Psi^{(\bar{p})}(\vec{x} + \vec{e}_i h) \left[(D+4) - \frac{e_i^2}{c_s^2} \right] \vec{e}_i, \quad (57)$$

$$\partial_{\vec{x}} \partial_{\vec{x}}^2 \Psi^{(\bar{p})} = \frac{1}{c_s^4} \sum_i w_i \Psi^{(\bar{p})}(\vec{x} + \vec{e}_i h) \left[\frac{e_i^2}{c_s^2} - (D+2) \right] \vec{e}_i. \quad (58)$$

In the discretization of the derivative terms two lattice stencils are used as a comparison, the D2Q9 described in Sec. II and the D2V141. The values of \vec{e}_i e w_i , for lattice stencil D2V141 are presented in Table I and $c_s = 1.194856755$.

Notice that when $a^{(p\bar{p})} = c_s^2 G^{(p\bar{p})}$ and $\kappa^{(p\bar{p})} = \frac{1}{2} c_s^4 G^{(p\bar{p})}$, the Eqs. (56)–(58) recover the force model originally proposed Shan and Chen [1].

In cases where vectors \vec{e}_i point to a solid node or a position outside the domain, especially for nodes near walls or boundaries of the domain, a specific approach is required for

TABLE I. Values of D2V141 lattice stencil vector groups and weights; p is the velocity vector count, obtained by permuting the vector x - and y - components.

\vec{e}_i	p	w_i
(0,0)	1	$1.1508949125706189 \times 10^{-1}$
($\pm 1, 0$)	4	$7.5595334899625166 \times 10^{-2}$
($\pm 1, \pm 1$)	4	$5.7734363121950370 \times 10^{-2}$
($\pm 2, 0$)	4	$2.9033095241565582 \times 10^{-2}$
($\pm 2, \pm 1$)	8	$1.8074672747613353 \times 10^{-2}$
($\pm 2, \pm 2$)	4	$7.4435479269746455 \times 10^{-3}$
($\pm 3, 0$)	4	$4.2549928887228462 \times 10^{-3}$
($\pm 3, \pm 1$)	8	$3.7759145451527918 \times 10^{-3}$
($\pm 3, \pm 2$)	8	$9.5510661516062627 \times 10^{-4}$
($\pm 4, 0$)	4	$4.9926973701248283 \times 10^{-4}$
($\pm 4, \pm 1$)	8	$2.1766901272228135 \times 10^{-4}$
($\pm 3, \pm 3$)	4	$2.7427360033189315 \times 10^{-4}$
($\pm 4, \pm 2$)	8	$1.3852638332696371 \times 10^{-4}$
($\pm 5, 0$)	4	$1.2905073342509215 \times 10^{-5}$
($\pm 4, \pm 3$)	8	$5.9323648903820310 \times 10^{-6}$
($\pm 5, \pm 1$)	8	$1.6161185887309810 \times 10^{-5}$
($\pm 5, \pm 2$)	8	$2.4159493337948245 \times 10^{-6}$
($\pm 4, \pm 4$)	4	$3.3101853527875648 \times 10^{-6}$
($\pm 5, \pm 3$)	8	$1.3086410701892049 \times 10^{-6}$
($\pm 6, 0$)	4	$1.1118416570950374 \times 10^{-7}$
($\pm 6, \pm 1$)	8	$4.6121305137932601 \times 10^{-7}$
($\pm 6, \pm 3$)	8	$3.6530518727364592 \times 10^{-8}$
($\pm 7, 0$)	4	$8.3273853753395782 \times 10^{-9}$
($\pm 7, \pm 2$)	8	$2.3109247814347261 \times 10^{-9}$

the calculation of derivative terms. We employ a symmetric reflection, denoted by $\vec{e}_i = -\vec{e}_i$ in the Eqs. (57) and (58). As

$$\partial_t \rho^{(p)} + \partial_{\vec{x}} \cdot \rho^{(p)} \vec{u} + \partial_{\vec{x}} \cdot (D_m \vec{m}_{(1)}^{(p)}) = 0, \quad (62)$$

$$\partial_t \rho + \partial_{\vec{x}} \cdot \rho \vec{u} = 0, \quad (63)$$

$$\partial_t (\rho^{(p)} \vec{u}) + \partial_{\vec{x}} \cdot \left(\rho^{(p)} \vec{u} \vec{u} - \rho^{(p)} \nu \left(\partial_{\vec{x}} \vec{u} + (\partial_{\vec{x}} \vec{u})^T - \frac{2}{D} (\partial_{\vec{x}} \cdot \vec{u}) I \right) \right) + \chi^{(p)} \partial_{\vec{x}} \cdot \mathbf{P} = -\partial_{\vec{x}} \cdot (D_m \mathbf{\Lambda}_m^{(p)}) + \rho^{(p)} \vec{g}^e, \quad (64)$$

$$\partial_t (\rho \vec{u}) + \partial_{\vec{x}} \cdot (\rho \vec{u} \vec{u} + \mathbf{P} - \rho \nu (\partial_{\vec{x}} \vec{u} + (\partial_{\vec{x}} \vec{u})^T)) = \rho \vec{g}^e, \quad (65)$$

where \mathbf{P} is the pressure tensor, Π^{neq} is the viscous stress tensor, $D_m = 1 - 1/(2\hat{\tau}_m) = 1/2$ (i.e., $\hat{\tau}_m = 1$) is the parameter that controls the intensity of the mixing process, $\mathbf{\Lambda}_m^{(p)}$ is the traceless tensor of inertia diffusivity given by

$$\mathbf{\Lambda}_m = \left(\vec{u} \vec{m}_{(1)}^{(p)} + (\vec{u} \vec{m}_{(1)}^{(p)})^T - \frac{2\vec{u} \cdot \vec{m}_{(1)}^{(p)}}{D} I \right), \quad (66)$$

and $\vec{m}_{(1)}^{(p)}$ is given by

$$\begin{aligned} \vec{m}_{(1)}^{(p)} &= \hat{\tau}_m (\chi^{(p)} \partial_{\vec{x}} \cdot \mathbf{P} - \partial_{\vec{x}} (c_s^2 \rho^{(p)}) + \rho^{(p)} (g_\alpha^{(p)} - g_\alpha^e)) \\ &= \hat{\tau}_m (\chi^{(p)} \partial_{\vec{x}} \cdot \mathbf{P} - \partial_{\vec{x}} \cdot \mathbf{P}^{(p)}). \end{aligned} \quad (67)$$

For details of the Chapman-Enskog analysis see the Appendix.

a result, this reflection leads to a null contribution from that symmetric direction.

G. Lattice Boltzmann and macroscopic equations

Defined the discretization schemes that were applied to the original pseudopotential model proposed Shan and Chen [1], the present model is characterized by the lattice Boltzmann equation:

$$\hat{f}_i^{(p)'} = f_{\text{eq},i}^{(p)} + \left(1 - \frac{1}{\hat{\tau}}\right) \hat{f}_{\text{neq},i}^{(p)} + \left(1 - \frac{1}{2\hat{\tau}}\right) F_i^{(p)} \delta_t, \quad (59)$$

where $\hat{f}_i^{(p)'} = \hat{f}_i^{(p)}(\vec{x} + \vec{e}_i \delta_t, t + \delta_t)$. In Eq. (59), we propose the utilization of an alternative smoothed equation for the term $\hat{\tau}$, which represents the relaxation time of the mixture

$$\hat{\tau} = \sum_p \tau^{(p)} (\chi^{(p)})^{\frac{\sum_{\bar{p}} \rho^{(\bar{p})}}{\rho^{(p)}}}. \quad (60)$$

The characteristic force per unit of mass (Eq. 23) which describes the pseudopotential is replaced by

$$\vec{g}^{(p)} = \vec{g}^e + \frac{\Psi^{(p)}}{\rho^{(p)}} \sum_{\bar{p}} (a^{(p\bar{p})} \partial_{\vec{x}} \Psi^{(\bar{p})} + \kappa^{(p\bar{p})} \partial_{\vec{x}}^2 \Psi^{(\bar{p})}), \quad (61)$$

where the parameter $G^{(p\bar{p})}$ is substituted by the parameters $a^{(p\bar{p})}$ and $\kappa^{(p\bar{p})}$ related to the control of the fluids immiscibility and interfacial forces, respectively, and both are considered equal for all fluids involved, i.e., $a^{(p\bar{p})} = a^{(\bar{p}p)}$ and $\kappa^{(p\bar{p})} = \kappa^{(\bar{p}p)}$.

Applying the Chapman-Enskog analysis in Eq. (59) to retrieve the macroscopic equations, the present model retrieves the equations of mass conservation and momentum balance in the form

The pressure tensor in the present model is represented by

$$\mathbf{P} = P_s \mathbf{I} + S, \quad (68)$$

where the scalar pressure is

$$P_s = P_e - \frac{1}{2} \sum_{p,\bar{p}} \kappa^{(p\bar{p})} (\partial_{\vec{x}}^2 (\Psi^{(p)} \Psi^{(\bar{p})}) - \partial_{\vec{x}} \Psi^{(p)} \cdot \partial_{\vec{x}} \Psi^{(\bar{p})}), \quad (69)$$

the thermodynamic pressure is

$$P_e = \rho c_s^2 - \frac{1}{2} \sum_{p,\bar{p}} a^{(p\bar{p})} \Psi^{(p)} \Psi^{(\bar{p})}, \quad (70)$$

and the interface tension or Korteweg tensor is

$$S = \sum_{p, \bar{p}} \kappa^{(p\bar{p})} (\partial_{\bar{x}} \Psi^{(p)} \partial_{\bar{x}} \Psi^{(\bar{p})}). \quad (71)$$

In the current model, the virtual mass denoted as $\Psi^{(p)}$ is assumed to be equal to $\rho^{(p)}$. As a result, the interaction between components algebraically consists of a simplified form of the Eq. (4) where the interactions into the same component ($p - p$) are not considered. In contrast, the Eq. (4) represents a model of attractive forces between the components with repulsive forces represented by the full Enskog's volume correction [Eq. (2)], while the original pseudopotential model and the present model [Eqs. (23) and (61)] describe repulsive forces between components. This representation of the system just by the repulsion between the components is inconsistent with the description of the molecular interaction behaviors, however, it proves to be an interesting tool in multicomponent models for representing complex engineering problems.

Comparing the mass and momentum balance equations, Eqs. (28)–(31) and (62)–(65), it can be seen that errors resulting from the force and mass diffusion terms have been eliminated. The force term errors were directly addressed by expliciting the force term and implementing the second-order discretization of the streaming term. Additionally, the diffusion term errors were corrected by reinterpreting the relaxation time [described by Eq. (60)].

V. RESULTS AND DISCUSSION

To examine the feasibility resulting from the discretization schemes applied, the two-dimensional cases of static bubble, two-components Poiseuille flow, and fluid displacement are simulated and compared with other works. The static bubble case is simulated using the lattices D2Q9 and D2V141 in the discretization of spatial derivative terms (defined in Sec. IV F) to compare their influences on the present model. The other cases are simulated using the D2V141 in the discretization of spatial derivative terms.

A. Static bubble

Aiming to verify the surface tension, spurious current, and its viscosity dependencies, simulations of the static bubble problem are performed using different viscosities and viscosity ratios. The problem geometry consists of a circular bubble of ratio r_b (fluid 2) located at the center of a square domain with length $H = 100 \text{ l.u}$ (lattice units) containing another suspension (fluid 1). Periodic conditions are applied on all boundaries (see Fig. 1). The problem considerations are those of steady regime, constant temperature, and null gravitational force, being both fluids incompressible and Newtonian. The flow steady-state regime is assumed when the L_2 error defined by

$$L_2 = \sqrt{\frac{\sum_{\bar{x}} [(u_x(\bar{x}, t) - u_x(\bar{x}, t-1))^2 + (u_y(\bar{x}, t) - u_y(\bar{x}, t-1))^2]}{\sum_{i,j} [(u_x(\bar{x}, t-1))^2 + (u_y(\bar{x}, t-1))^2]}}, \quad (72)$$

reaches a value less than 10^{-10} .

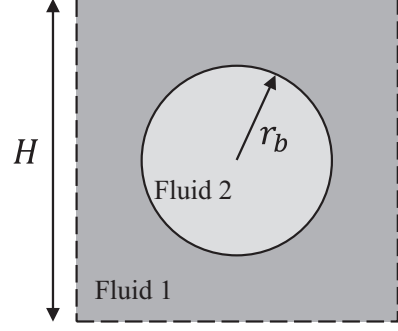


FIG. 1. Schematic representation of the static bubble problem. Fluid 2 represents the bubble, fluid 1 is the suspension fluid, H is the domain height, and r_b is the bubble ratio.

Analyzing the model dependencies in relation to the fluid viscosity parameter, the behaviors of stability, spurious currents, and surface tension are observed for variations of the viscosity ratio, defined by

$$M_v = \frac{\nu_1}{\nu_2}. \quad (73)$$

Before any specific analysis, an immiscibility test is required. We measure the influence of the $a_{\sigma\bar{\sigma}}$ coefficient to estimate the miscibility and immiscibility ranges. In this test, densities of fluid 2 (ρ_2) and fluid 1 (ρ_1) are monitored at the center of the volume with $r_b = 40 \text{ l.u}$, also M_v is varied by setting $\rho_1 = \rho_2 = 1$, $\kappa_{\sigma\bar{\sigma}} = 0$, and $\nu_1 = 0.78125$. In the results obtained for the range of $a_{\sigma\bar{\sigma}}$ shown in Fig. 2, values of $a_{\sigma\bar{\sigma}} \leq 0.7$ represent the diffusion of one fluid over the other, the interval $0.7 < a_{\sigma\bar{\sigma}} \leq 1.0$ indicates a transition range of the fluid interaction, and with a certain tolerance, values $1.0 \leq a_{\sigma\bar{\sigma}}$ represents immiscibility range. Additionally, the behavior of the components remains independent of variations in M_v within the transition region and immiscibility range, while varying $a_{\sigma\bar{\sigma}}$.

Comparing lattice stencils, less stability was observed in the variation of $a_{\sigma\bar{\sigma}}$ for D2Q9, with numerical instability for

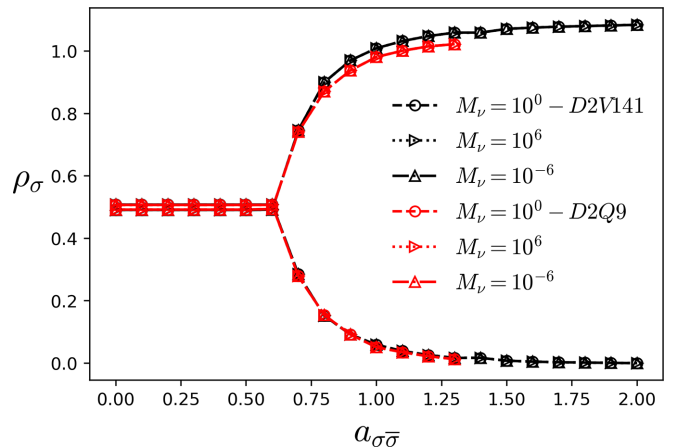


FIG. 2. Immiscibility test range varying the viscosity ratio: the lines in the red and black color are the results obtained for the lattices D2Q9 and D2V141, respectively.

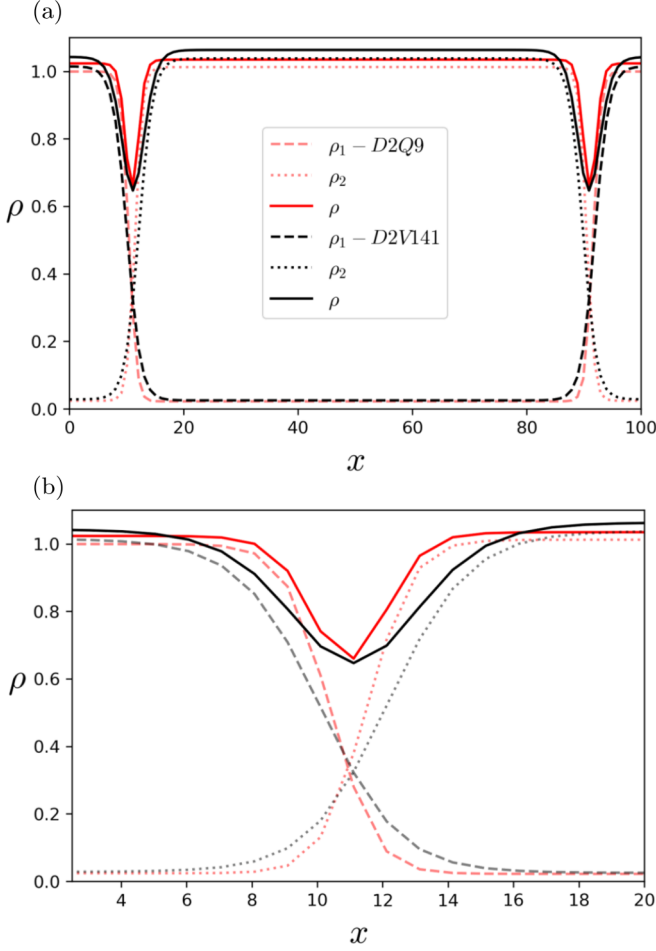


FIG. 3. Comparison of the density profile of the D2Q9 stencil (red) with that of the D2V141 (black): (a) density profiles along x and $y = H/2$; (b) zoom image of the interface transition.

$a_{\sigma\bar{\sigma}} > 1.3$ and $a_{\sigma\bar{\sigma}} > 2.0$ for D2Q9 and D2V141, respectively. For the same values of $a_{\sigma\bar{\sigma}}$, the D2V141 stencil presented density values higher than the D2Q9. Such values refer to the transition interface between the components that tend to create a lower density region [Fig. 3(b)] that consequently increases the maximum density values of each component. Figure 3 illustrates this behavior in the interface transition by plotting the density values obtained in x for $y = H/2$ and $a_{\sigma\bar{\sigma}} = 1.2$.

Once the immiscibility range is defined, the analysis of interfacial tension between immiscible fluids 1 and 2 relies on the Laplace equation, with r_b varying as a function of Δp :

$$\Delta p = p_2 - p_1 = \frac{\gamma}{r_b}. \quad (74)$$

The physical representation of interfacial tension (γ) is verified by the present model varying M_v , $a_{\sigma\bar{\sigma}}$, and $\kappa_{\sigma\bar{\sigma}}$. The results shown in Fig. 4 demonstrate an approximately linear relationship between Δp and $1/r_b$, as well as a relative independence of γ from M_v and a proportionate increase in γ with increasing values of $a_{\sigma\bar{\sigma}}$ and $\kappa_{\sigma\bar{\sigma}}$. Consequently, the proposed force model with $a_{\sigma\bar{\sigma}}$ and $\kappa_{\sigma\bar{\sigma}}$ allows improved control of the parameters that affect the interface region and interfacial tension for the lattice D2V141. For the lattice D2Q9, the variation of $\kappa_{\sigma\bar{\sigma}}$ with respect to $a_{\sigma\bar{\sigma}}$ has no effect on the interfacial

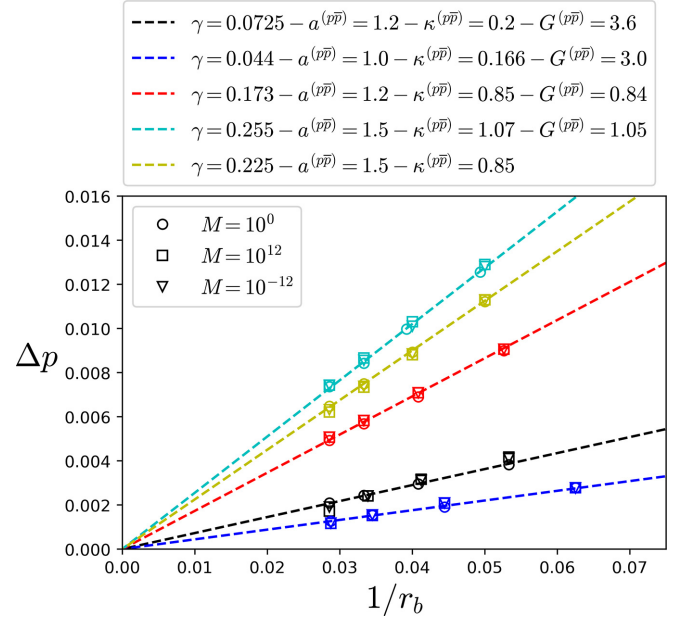


FIG. 4. Interfacial tension: Laplace equation verification for different values of M_v , $a_{\sigma\bar{\sigma}}$ and $\kappa_{\sigma\bar{\sigma}}$.

tension. In addition, as highlighted in Fig. 4, viscosity ratio values was simulated in the range of $M_v = 10^{12}$, 10^0 , and 10^{-12} for $\nu_1 = 3.86 \times 10^{11}$, 3.86×10^{-1} , and 3.86×10^{-13} , respectively.

Investigating the influence of spurious currents on the model, we perform a specific formulation of the static bubble problem, as used in the works of Otomo *et al.* [11], Porter *et al.* [16], Gharibi and Ashrafizaadeh [19], to analyze the maximum magnitude of spurious currents, $|u|_{\max}$, in relation to viscosity and viscosity ratio. In the formulation, we consider $H = 62$, $r_b = 24$, and choose the parameter values of the force model at the onset of the immiscibility range, which corresponds to $a_{\sigma\bar{\sigma}} = 1.0$ and the respective value of $\kappa_{\sigma\bar{\sigma}}$ following the proportion of $G_{\sigma\bar{\sigma}}$. The results obtained for both test types can be seen in Figs. 5(a) and 5(b).

Figure 5(a) shows results for the test of varying ν_1 for fixed $M_v = 1$; the model currently proposed demonstrates that $|u|_{\max}$ decreases as viscosity increases until reaching approximately constant values of mid- $O(10^{-4})$ and of upper- $O(10^{-5})$ lattice units for the D2Q9 and D2V141 formulation stencils, respectively.

On the other hand, maintaining constant $\nu_1 = 0.0067$ while varying M_v , as shown in Fig. 5(b), one can observe a decrease of $|u|_{\max}$ with increasing viscosity ratio until reaching approximately constant values of upper- $O(10^{-4})$ and upper- $O(10^{-5})$ lattice units for the D2Q9 and D2V141 formulation stencils, respectively. Compared to the models presented in the works of Porter *et al.* [16], Otomo *et al.* [11], and Gharibi and Ashrafizaadeh [19], the model herein proposed demonstrates a significantly wider stability range and relatively smaller values of $|u|_{\max}$, for both cases of extreme individual ν_1 and M_v values, reaching magnitudes of about upper- $O(10^{-5})$ lattice units values. It is important to note that in their studies, Porter *et al.* [16] and Gharibi and Ashrafizaadeh [19] utilized the tenth-order isotropy scheme proposed by Sbragaglia *et al.* [36] for discretizing derivative terms.

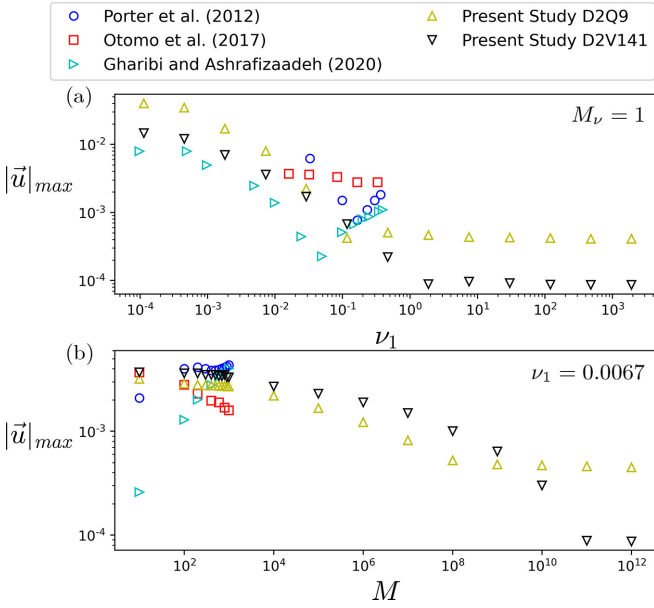


FIG. 5. Spurious currents analysis: $|u|_{max}$ magnitude values as a function of (a) ν_1 for $M_v = 1$ and (b) viscosity ratio M_v for $\nu_1 = 0.0067$.

Regarding the numerical stability of the problem as a function of the viscosity ratio, no limit value for which the simulation becomes unstable occurred, which makes it possible to simulate the viscosity ratio tending to zero and infinity. However, the computational time required to achieve the steady regime tends to increase with the values of the viscosity ratio tending to the extremes. On the other hand, in terms of the force model discretization, the D2V141 stencil presents greater stability in the variation $a_{\sigma\bar{\sigma}}$, better control of the interfacial tension, besides the already mentioned relatively lower values of spurious currents.

B. Two-components Poiseuille flow

To evaluate the improvements in the proposed model for a dynamic problem, numerical results are compared with the analytical solution for the two-components Poiseuille flow. Details of the analytical solution can be seen in Porter *et al.* [16]. The problem geometry is a channel of length $L = 7 l.u$ and high $2H = 300 l.u$ with two fluid components. Fluid 1 flows in the central region of the channel (height $2a$), while fluid 2 flows bounded by the channel walls, as illustrated in Fig. 6. The boundary conditions are nonslip on the walls applied by the mass conservative Method II presented in the work of Bazarin *et al.* [37] and periodicity at the inlet and outlet of the channel. The flow is promoted by a pressure gradient inserted as an external force. The problem's assumptions include a constant temperature, negligible gravitational force, and the assumption that both fluids are incompressible and Newtonian. Simulations are performed up to the steady-state regime where, according to Eq. (72), the error reaches 10^{-10} .

Considering $\rho_1 = \rho_2 = 1$, $a = 75$, $a_{\sigma\bar{\sigma}} = 1.2$ and $\kappa_{\sigma\bar{\sigma}} = 0$, Fig. 7 depicts a comparison between the numerical and analytical results of the velocity profile for (a) $M_v = 10^{-1}$, (b) $M_v = 10^1$, (c) $M_v = 10^{-6}$ and (d) $M_v = 10^6$. The velocity

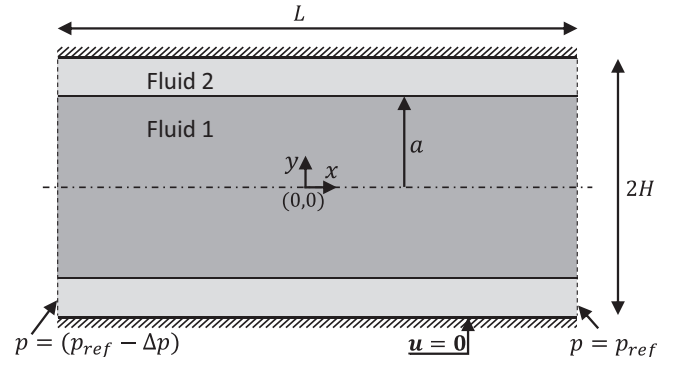


FIG. 6. Schematic representation of the two-components Poiseuille flow problem.

profiles are normalized by the analytical maximum velocity. $\kappa_{\sigma\bar{\sigma}}$ is set to 0 to reduce the interface spacing between components. In the simulated cases, the fluid 1 viscosity for $M_v > 1$ and $M_v < 1$ is fixed at $\nu_1 = 909.42$ and $\nu_1 = 0.018188$, respectively.

Varying the height a to $a_{\sigma\bar{\sigma}} = 1.2$ and $\kappa_{\sigma\bar{\sigma}} = 0.0$, the numerical and analytical relative permeability results ($k_{r\sigma}$) in function of the fluid 2 saturation ($S_2 = 1 - a/H$) are illustrated in Figs. 8(a) for $M_v > 0$ and 8(b) for $M_v < 0$. The analytical solution for the relative permeability can be seen in Porter *et al.* [16]. The results are presented for $a/H = 0.9, 0.75, 0.5, 0.33, 0.2$ and viscosity ratio varying in $10^{-5} \leq M_v \leq 10^5$. A quantitative comparison of the results is shown in Fig. 8 can be seen in Table II.

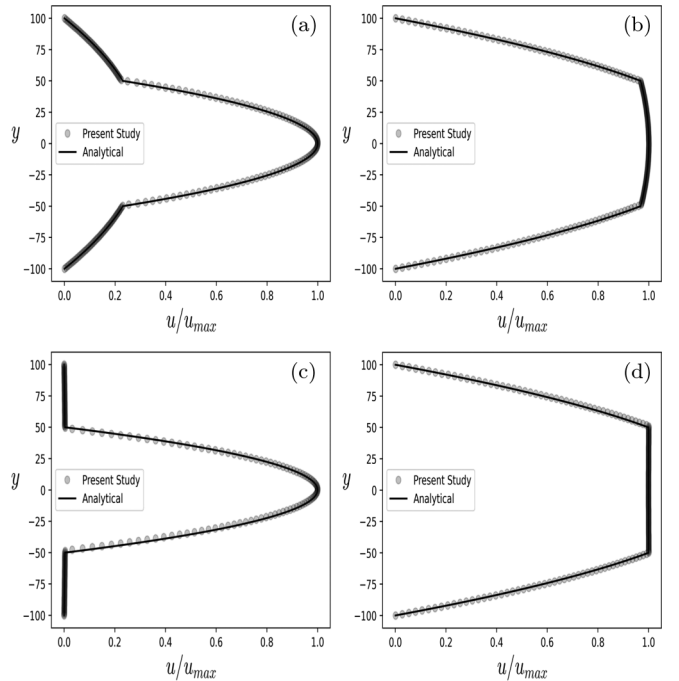


FIG. 7. Comparison between numerical (dots) and analytical (lines) velocity profiles: (a) 10^{-1} , (b) 10^1 , (c) 10^{-6} , (d) 10^6 . In each case, the velocities plotted are normalized by the maximum analytical velocity u_{max} .

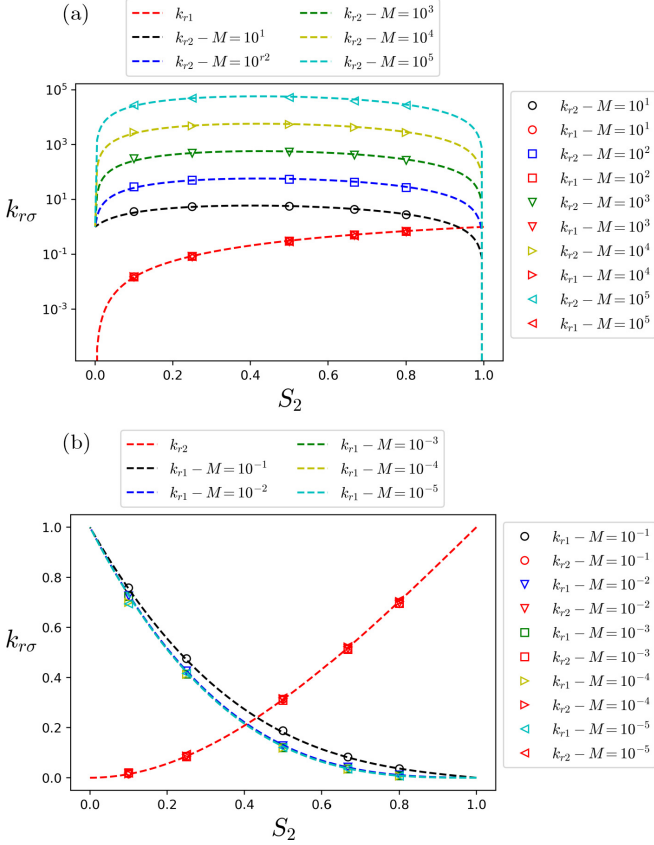


FIG. 8. Comparison between numerical and analytical results of relative permeability (k_{rp}) for (a) $M_v > 10^0$ and (b) $M_v < 10^0$.

The errors between the numerical and analytical relative permeability can be seen in Table II. The root-mean-squared error and maximum relative percent error are calculated and compared to the values presented by Porter *et al.* [16]. The results demonstrate a tendency to increase errors with the increase of M_v to $M_v > 10^0$ and the decrease of M_v to $M_v < 10^0$. However, all errors observed are in the order of 10^0 , similar to the errors obtained by Porter *et al.* [16].

TABLE II. Relative permeability errors after comparison with Porter *et al.* [16].

M_v	RMSE				MRPE%			
	k_{r1}		k_{r2}		k_{r1}		k_{r2}	
	P.W.	[16]	P.W.	[16]	P.W.	[16]	P.W.	[16]
10^{-5}	0.015	–	0.011	–	10.679	–	10.97	–
10^{-4}	0.014	–	0.002	–	9.224	–	10.34	–
10^{-3}	0.005	–	0.005	–	6.459	–	9.44	–
10^{-2}	0.002	0.002	0.003	0.017	4.779	6.6	8.965	5.4
10^{-1}	0.004	0.010	0.004	0.013	1.903	3.7	3.448	5.1
10^1	0.166	0.086	0.007	0.008	2.482	4.4	5.512	3.9
10^2	1.161	1.73	0.009	0.012	4.693	6.6	3.443	4.8
10^3	30.45	–	0.017	–	7.863	–	5.277	–
10^4	125.2	–	0.022	–	8.301	–	5.324	–
10^5	2753.2	–	0.043	–	9.234	–	9.854	–

Similarly to the static bubble problem, there is no instability limiting the range of viscosity ratio. However, for a fixed mesh (h) and time step (δ_t), the numerical precision decreases as the viscosity ratio values tend to the extremes, being necessary to refine the mesh and the time step to maintain accuracy.

C. Fluid-fluid displacement

The last case analyzed is the transient problem of fluid-fluid displacement in a channel, where patterns of fingering formation can be analyzed according to the parameters of viscosity ratio and capillary number. The problem is characterized by one fluid that is injected displacing another fluid initially present in the channel of length L and height H . Figure 9 illustrates the initial conditions and boundary conditions of the problem. Initially, fluid 2 fills a rectangular region of $L_2 \times H$ at the inlet of the channel, while fluid 1 fills the remaining region of $L_1 \times H$, with both fluids having null initial velocity. At the inlet and outlet of the channel, boundary conditions for the developed velocity (parabolic profile) are applied, and nonslip conditions are applied to the upper and lower walls. All boundaries are implemented using the mass conservative Method II presented in the work Bazarin *et al.* [37]. The problem is assumed to be at a constant temperature with negligible gravitational force, and both fluids are considered to be incompressible and Newtonian.

In the simulations, the values of H , L_1 , and L_2 are 100, 10, and 590 $l.u.$, respectively. The force model parameters are $a_{\sigma\bar{\sigma}} = 1.2$ and $\kappa_{\sigma\bar{\sigma}} = 0.85$ corresponding to $\gamma = 0.255$. Figure 10 shows results for different values of viscosity ratio, simulated by varying the capillary number, which is defined as

$$Ca = \frac{U_{\max} \nu_1}{\gamma}, \quad (75)$$

where U_{\max} is maximum velocity of parabolic profile. The fingering patterns, obtained for $M_v = 10^4$ and $\nu_1 = 1.25 \times 10^{-4}$ at different values of Ca , show the contours corresponding to the Atwood number $(\rho_1 - \rho_2)/(\rho_1 + \rho_2)$ at the point where the finger reaches a length of 550 $l.u.$.

To analyze the patterns presented in Fig. 10, the measurements of finger length in the simulated cases are compared with the Halpern and Gaver III [38] correlation:

$$\frac{a_f}{H} = 1 - 4.17(1 - e^{-1.69Ca^{0.5025}}). \quad (76)$$

where the finger width (a_f), normalized by the channel height (H), is predicted as a function of the flow capillary number (Ca). Figure 11 illustrates the agreement between Eq. (76) and the numerical results for varying values of M_v , specifically 10^1 , 10^2 , 10^3 , and 10^4 . The constant error bar of $\pm 4 l.u.$ serves to characterize the interface length.

While instabilities associated with M_v are absent in the previous scenarios, they become noticeable in the context of fluid displacement when $M_v \geq 10^5$. Moreover, within this same range of M_v , there is an observable trend of increased occurrence of spurious currents, which impacts the formation of fingering patterns. Notably, in comparison to the model

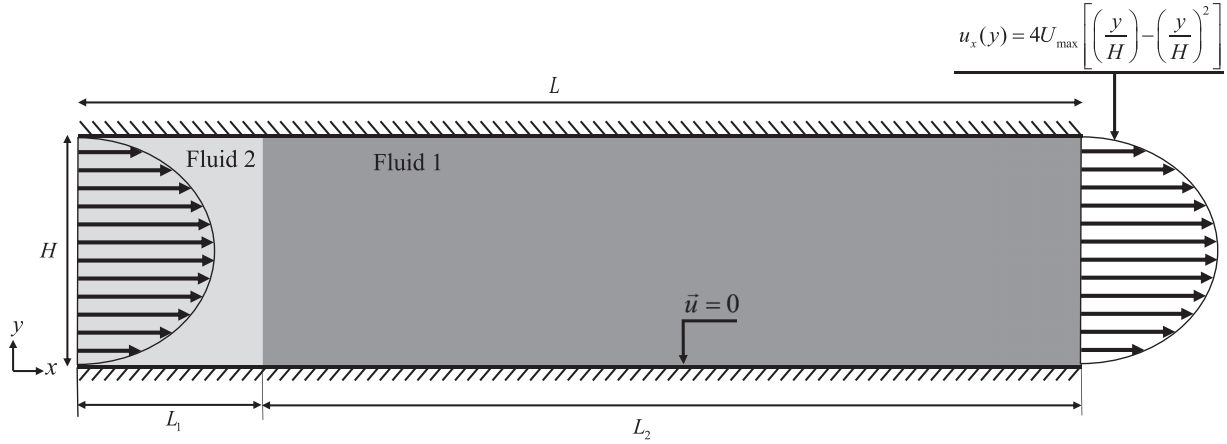


FIG. 9. Problem of fluid-fluid displacement: Geometry, initial, and boundary conditions.

proposed by Otomo *et al.* [11], this study extends the range of M_v from 10^2 to 10^4 .

VI. CONCLUSIONS

In the present work, a multicomponent model focusing on the viscosity gradient at the fluid interface was studied. The model was developed as an improved pseudo-potential model based on the application of different models and discretization schemes, which control moments present in the problem formulation and minimize spurious terms resulting from the discretization process.

Specifically in the analysis of the results, excellent applicability of the model was observed for problems with high viscosity ratios. In the static bubble problem, a correct

representation and fine control of the interface region were observed with the proposed force model. In the analysis of the maximum magnitude of spurious currents were observed values in the range of upper- $O(10^{-2})$ and upper- $O(10^{-5})$ lattice units.

For the dynamic two-components Poiseuille flow problem, a correct representation of the viscous coupling was observed by the proposed smooth viscosity equation at the interface, as well as good accuracy in comparison with the analytical results. In both problems, static bubble and two-components Poiseuille flow, instabilities were not observed for viscosity ratios tending to both extremes (zero and infinite). Finally, for the transient fluid-fluid displacement problem a correct representation of the finger patterns and excellent proximity to the Halpern and Gaver III [38] correlation was observed. However, in contrast to the previous problems instability was observed for viscosity ratios greater than 10^4 .

In comparison with other works focused on the representation of the viscosity gradient for the pseudo-potential model, specifically Porter *et al.* [16], Otomo *et al.* [11], and Gharibi and Ashrafizaadeh [19], the present model demonstrates stability ranges for extremely higher viscosity ratios and similar

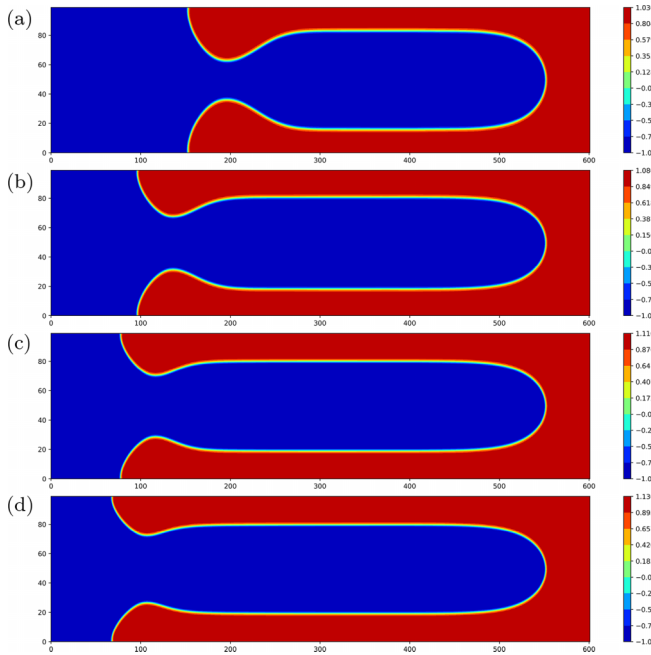


FIG. 10. Fingering patterns obtained for $M_v = 10^4$, $\nu_1 = 1.25 \times 10^{-4}$ and (a) $Ca = 0.6$, (b) $Ca = 1.1$, (c) $Ca = 1.6$, and (d) $Ca = 2.1$.

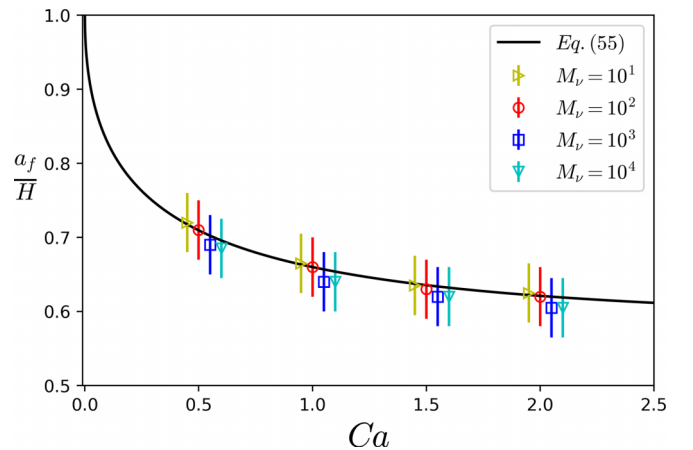


FIG. 11. Normalized finger width (a_f/H) as a function of the capillary number (Ca): comparison with Eq. (76) for different viscosity ratios.

control of other parameters such as interfacial tension and spurious currents.

Nevertheless, some drawbacks of the present model must be addressed or minimized to improve and extend the applicability for other complex problems in immiscible multicomponent systems. The main drawbacks are the relatively high values of spurious currents and the inability of the force model to represent interactions of immiscible fluids with different densities. In this sense, a more direct LB representation of Eq. (1), as briefly presented by Eq. (5), proves to be a promising path for the improvement of the present model. However, the current model holds potential for representing multicomponent fluid flow through complex geometries. An example is fluid displacement through porous media. Exploring this application will be the next step in our research.

APPENDIX: SCALE ANALYSIS OF THE LB EQUATION

The scale analysis of the LB equation to retrieve the macroscopic equations is performed using a Chapman-Enskog analysis, based on an asymptotic expansion of the distribution function f in terms of the Knudsen number $\varepsilon = \ell/L$, ℓ being used to represent the mean free path and L a macroscopic characteristic length.

Before the expansion process, a scale analysis of the Boltzmann equation is performed to quantify the order of magnitude of the several terms in the Boltzmann equation. Considering τ to be the molecular collision time scale, Γ the macroscopic time scale, $\bar{\xi} = \sqrt{kT_0/m} = \ell/\tau$ the mean molecular speed (where k is the Boltzmann constant, T_0 a reference temperature and m the molecular mass), we have the dimensionless quantities:

$$t = \frac{t^*}{\Gamma}, \quad \bar{x} = \frac{x^*}{L}, \quad \bar{\xi} = \frac{\xi^*}{\bar{\xi}}, \quad \bar{g}^e = \frac{g_e^* \Gamma}{\bar{\xi}},$$

$$f^{(p)} = \frac{f_p^* \bar{\xi}^D}{\rho_0}, \quad \Omega^{(p)} = \frac{\Omega_p^* \bar{\xi}^D}{\rho_0 \tau}, \quad (\text{A1})$$

where (*) indicates the dimensional quantities and $\Omega^{(p)} = \sum_{s=1}^r \Omega^{ps}$. Therefore, the continuous Boltzmann equation becomes

$$\frac{\chi}{\varepsilon} (\partial_t f^{(p)} + \bar{\xi} \cdot \partial_{\bar{x}} f^{(p)} + \bar{g}^e \cdot \partial_{\bar{\xi}} f^{(p)}) = \frac{\Omega^{(p)}}{\varepsilon}, \quad (\text{A2})$$

$\chi = \tau/\Gamma$ being the ratio between the scales of time. In Eq. (A2) the collision term is dominant when $\ell \ll L$ and $\tau \ll \Gamma$ [39]. Consequently, the ratio χ/ε is $\mathcal{O}(1)$ and $\bar{\xi} = \ell/\tau \approx L/\Gamma$.

1. Chapman-Enskog analysis: Pseudopotential

Expanding the term $\hat{f}_i^{(p)}(\bar{x} + \bar{e}_i \delta_t, t + \delta_t)$ in Eq. (20) in Taylor series, we obtain

$$\sum_{j=1}^{\infty} \frac{\chi^j}{\varepsilon} \frac{1}{j!} D_t^j \hat{f}_i^{(p)} = -\frac{1}{\varepsilon} \frac{\hat{f}_i^{(p)} - \hat{f}_{\text{eq},i}^{(p)}}{\tau^{(p)}} + F_i^{(p)}, \quad (\text{A3})$$

in the nondimensional scale. Expanding asymptotically the distribution function f and the time derivative ∂_t ,

$$\hat{f}_i^{(p)} = \sum_{k=0}^{\infty} \varepsilon^k \hat{f}_{i,p}^{(k)} = \hat{f}_{i,p}^{(0)} + \varepsilon \hat{f}_{i,p}^{(1)} + \varepsilon^2 \hat{f}_{i,p}^{(2)} + \dots,$$

$$\partial_t = \sum_{k=0}^{\infty} \partial_t^{(k)} = \partial_t^{(0)} + \varepsilon \partial_t^{(1)} + \varepsilon^2 \partial_t^{(2)} + \dots, \quad (\text{A4})$$

where ε^k represents the order of the Knudsen number. Replacing the expanded terms in Eq. (A3) and separating the terms by order of the Knudsen number up to $\mathcal{O}(\varepsilon)$, we have

$$O(\varepsilon^{-1}) : \hat{f}_{i,p}^{(0)} = \hat{f}_{i,\text{eq}}^{(p)}(\rho^{(p)}, \vec{u}'),$$

$$O(\varepsilon^0) : D_t^{(0)} \hat{f}_{i,p}^{(0)} = -\frac{\hat{f}_{i,p}^{(1)}}{\tau^{(p)}} + F_i^{(p)},$$

$$O(\varepsilon) : \partial_t^{(1)} \hat{f}_{i,p}^{(0)} + D_t^{(0)} \hat{f}_{i,p}^{(1)} + \frac{1}{2} D_t^{(0)2} \hat{f}_{i,p}^{(0)} = -\frac{\hat{f}_{i,p}^{(2)}}{\tau^{(p)}}, \quad (\text{A5})$$

or

$$O(\varepsilon) : \partial_t^{(1)} \hat{f}_{i,p}^{(0)} + D_t^{(0)} \left(\left(1 - \frac{1}{2\tau^{(p)}} \right) \hat{f}_{i,p}^{(1)} \right) + D_t^{(0)} \left(\frac{F_i^{(p)}}{2} \right) = -\frac{\hat{f}_{i,p}^{(2)}}{\tau^{(p)}}. \quad (\text{A6})$$

The mass conservation equation for the p component is retrieved at order ε^0 as

$$\partial_t^{(0)} \rho^{(p)} + \partial_{\bar{x}} \cdot (\rho^{(p)} \vec{u}') = 0, \quad (\text{A7})$$

and for the mixture

$$\partial_t^{(0)} \rho + \partial_{\bar{x}} \cdot (\rho \vec{u}') = 0. \quad (\text{A8})$$

The momentum balance equation for the p component

$$\partial_t^{(0)} (\rho^{(p)} \vec{u}') + \partial_{\bar{x}} \cdot (\rho^{(p)} c_s^2 + \rho^{(p)} \vec{u}' \vec{u}') = -\frac{\bar{m}_{(1)}^{(p)}}{\tau^{(p)}} + \rho^{(p)} \bar{g}^{(p)}, \quad (\text{A9})$$

and for the mixture

$$\partial_t^{(0)} (\rho \vec{u}') + \partial_{\bar{x}} \cdot (\mathbf{P}_{SC} + \rho \vec{u}' \vec{u}') = \rho \bar{g}^e, \quad (\text{A10})$$

where \mathbf{P}_{SC} is the pressure tensor given by Eq. (32). The first-order moment of nonequilibrium $\bar{m}_{(1)}^{(p)}$ in Eq. (36) is determined by Eqs. (A9) and (A10).

Extending for order ε^1 , we have the mass conservation equation for the p -component at this order

$$\partial_t^{(1)} \rho^{(p)} + \left(1 - \frac{1}{2\tau^{(p)}} \right) \partial_{\bar{x}} \cdot \bar{m}_{(1)}^{(p)} + \frac{1}{2} \partial_{\bar{x}} \cdot (\rho^{(p)} \bar{g}^{(p)}) = 0, \quad (\text{A11})$$

and for the mixture

$$\partial_t^{(1)} \rho + \sum_p \partial_{\bar{x}} \cdot \bar{m}_{(1)}^{(p)} + \sum_p \left(\frac{1}{2} \partial_{\bar{x}} \cdot \rho^{(p)} \bar{g}^{(p)} \right) = 0. \quad (\text{A12})$$

The momentum balance equation for the p component

$$\begin{aligned} \partial_t^{(1)} \rho^{(p)} \vec{u}' + \left(1 - \frac{1}{2\tau^{(p)}}\right) \partial_t^{(0)} \vec{m}_{(1)}^{(p)} + \left(1 - \frac{1}{2\tau^{(p)}}\right) \partial_{\vec{x}} \cdot \left(\vec{u}' \vec{m}_{(1)}^{(p)} + (\vec{u}' \vec{m}_{(1)}^{(p)})^T - \tau^{(p)} \rho^{(p)} (\partial_{\vec{x}} \vec{u}' + (\partial_{\vec{x}} \vec{u}')^T)\right) \\ + \frac{1}{2} \partial_t^{(0)} (\rho^{(p)} \vec{g}^{(p)}) + \frac{1}{2} \partial_{\vec{x}} \cdot \rho^{(p)} (\vec{g}^{(p)} \vec{u}' + (\vec{g}^{(p)} \vec{u}')^T + \tau^{(p)} \vec{g}^{(p)} \vec{g}^{(p)}) = 0, \end{aligned} \quad (\text{A13})$$

and the momentum balance equation for the mixture

$$\begin{aligned} \partial_t^{(1)} \rho \vec{u}' + \sum_p (\partial_t^{(0)} \vec{m}_{(1)}^{(p)}) + \sum_p \partial_{\vec{x}} \cdot \left(\vec{u}' \vec{m}_{(1)}^{(p)} + (\vec{u}' \vec{m}_{(1)}^{(p)})^T\right) - \sum_p \left(\left(\tau^{(p)} - \frac{1}{2}\right) \partial_{\vec{x}} \cdot \rho^{(p)} (\partial_{\vec{x}} \vec{u}' + (\partial_{\vec{x}} \vec{u}')^T)\right) \\ + \frac{1}{2} \partial_t^{(0)} \sum_p (\rho^{(p)} \vec{g}^{(p)}) + \sum_p \left(\frac{1}{2} \partial_{\vec{x}} \cdot \rho^{(p)} (\vec{g}^{(p)} \vec{u}' + (\vec{g}^{(p)} \vec{u}')^T + \tau^{(p)} \vec{g}^{(p)} \vec{g}^{(p)})\right) = 0, \end{aligned} \quad (\text{A14})$$

where the second-order moments of $\hat{f}_{i,p}^{(1)}$ are obtained from Eq. (A6).

Summing Eqs. (A7)–(A14), we recover the balance equations, Eqs. (28)–(31).

2. Present Model

Expanding $\hat{f}_i^{(p)}(\vec{x} + \vec{e}_i \delta_t, t + \delta_t)$ in a Taylor series, in Eq. (46)

$$\sum_{j=1}^{\infty} \frac{\chi^j}{\varepsilon} \frac{1}{j!} D_t^j \hat{f}_i^{(p)} = M^{-1} S M \left[\frac{\hat{f}_{\text{eq},i}^{(p)} - \hat{f}_i^{(p)}}{\varepsilon} - \frac{F_i^{(p)}}{2} \right] + F_i^{(p)}, \quad (\text{A15})$$

where M and S are given by the Eqs. (47) and (48), respectively.

On the other hand, the asymptotic expansion [Eq. (A4)] results in the following hierarchy of scales:

$$\begin{aligned} O(\varepsilon^{-1}) : \hat{f}_{i,p}^{(0)} &= \hat{f}_{i,\text{eq}}^{(p)}(\rho^{(p)}, \vec{u}), \\ O(\varepsilon^0) : D_t^{(0)} \hat{f}_{i,p}^{(0)} &= -\hat{f}_{i,p,S}^{(1)} - \frac{1}{2} F_{i,S}^{(p)} + F_i^{(p)}, \\ O(\varepsilon) : \partial_t^{(1)} \hat{f}_{i,p}^{(0)} + D_t^{(0)} \hat{f}_{i,p}^{(1)} + \frac{1}{2} D_t^{(0)2} \hat{f}_{i,p}^{(0)} &= -\hat{f}_{i,p,S}^{(2)}, \end{aligned} \quad (\text{A16})$$

or

$$\begin{aligned} O(\varepsilon) : \partial_t^{(1)} \hat{f}_{i,p}^{(0)} + D_t^{(0)} \left(\hat{f}_{i,p}^{(1)} - \frac{\hat{f}_{i,p,S}^{(1)}}{2} \right) + D_t^{(0)} \left(\frac{F_i^{(p)}}{2} - \frac{F_{i,S}^{(p)}}{4} \right) \\ = -\hat{f}_{i,p,S}^{(2)}, \end{aligned} \quad (\text{A17})$$

where $\hat{f}_{i,S_p}^{(1)}$ and $F_{i,S}^{(p)}$ are given by

$$\begin{aligned} \hat{f}_{i,p,S}^{(1)} &= M^{-1} S M \hat{f}_{i,p}^{(1)} \\ &= \omega_i \left[\frac{\vec{e}_i m_{(1)}^{(p)}}{\hat{\tau}_m c_s^2} + \frac{\Pi_{(1)}^{(p)} : (\vec{e}_i \vec{e}_i - c_s^2 \mathbf{I})}{2 \hat{\tau}_v c_s^2} - \frac{1}{2} F_{i,S}^{(p)} \right], \end{aligned} \quad (\text{A18})$$

$$\begin{aligned} F_{i,S}^{(p)} &= M^{-1} S M F_i^{(p)} \\ &= \omega_i \rho^{(p)} \left[\frac{\vec{e}_i \cdot \vec{g}^{(p)}}{\hat{\tau}_m c_s^2} + \frac{(\vec{u} \vec{g}^{(p)} + (\vec{u} \vec{g}^{(p)})^T) : (\vec{e}_i \vec{e}_i - c_s^2 \mathbf{I})}{2 \hat{\tau}_v c_s^2} \right], \end{aligned} \quad (\text{A19})$$

where $\hat{\tau}_v = \hat{\tau}_4 = \hat{\tau}_5$ and $\hat{\tau}_m = \hat{\tau}_1 = \hat{\tau}_2$.

The mass conservation equation is retrieved at order $\varepsilon^{(0)}$ as,

$$\partial_t^{(0)} \rho^{(p)} + \partial_{\vec{x}} \cdot (\rho^{(p)} \vec{u}) = 0, \quad (\text{A20})$$

and for the mixture

$$\partial_t^{(0)} \rho + \partial_{\vec{x}} \cdot (\rho \vec{u}) = 0. \quad (\text{A21})$$

The momentum balance equation for the p component is retrieved at order $\varepsilon^{(0)}$ as

$$\partial_t^{(0)} (\rho^{(p)} \vec{u}) + \partial_{\vec{x}} \cdot (\rho^{(p)} c_s^2 + \rho^{(p)} \vec{u} \vec{u}) = \frac{-\vec{m}_{(1)}^{(p)}}{\hat{\tau}_m} + \rho^{(p)} \vec{g}^{(p)}, \quad (\text{A22})$$

and for the mixture

$$\partial_t^{(0)} (\rho \vec{u}) + \partial_{\vec{x}} \cdot (\mathbf{P} + \rho \vec{u} \vec{u}) = \rho \vec{g}^e, \quad (\text{A23})$$

where \mathbf{P} is the pressure tensor given by Eq. (68), $\sum_i \hat{f}_i^{1(p)} \vec{e}_i = \vec{m}_{(1)}^{(p)} - \frac{1}{2} \sum_i F_i^{(p)} \vec{e}_i$, and $\sum_i \hat{f}_i^{1(p)} \vec{e}_i \vec{e}_i = \mathbf{\Pi}_{(1)}^{(p)} - \frac{1}{2} \sum_i F_i^{(p)} \vec{e}_i \vec{e}_i$. The first-order moment of non-equilibrium $\vec{m}_{(1)}^{(p)}$ is determined by the Eqs. (A22) and (A23), being described by Eq. (67).

Extending the order to $\varepsilon^{(1)}$, we have the mass conservation equation for the p component

$$\partial_t^{(1)} \rho^{(p)} + \partial_{\vec{x}} \cdot \left(\left(1 - \frac{1}{2\hat{\tau}_m}\right) \vec{m}_{(1)}^{(p)} \right) = 0, \quad (\text{A24})$$

and for the mixture

$$\partial_t^{(1)} \rho = 0, \quad (\text{A25})$$

the momentum balance equation for the p component

$$\begin{aligned} \partial_t^{(1)} \rho^{(p)} \vec{u} + \partial_t^{(0)} \vec{m}_{(1)}^{(p)} \\ + \partial_{\vec{x}} \cdot \left(\left(\hat{\tau} - \frac{1}{2} \right) c_s^2 \rho^{(p)} \left(\partial_{\vec{x}} \vec{u} + (\partial_{\vec{x}} \vec{u})^T - \frac{2}{D} (\partial_{\vec{x}} \cdot \vec{u}) \mathbf{I} \right) \right) \\ - \partial_{\vec{x}} \cdot \left(\left(1 - \frac{1}{2\hat{\tau}}\right) \left(\vec{u} \vec{m}_{(1)}^{(p)} + (\vec{u} \vec{m}_{(1)}^{(p)})^T - \frac{2\vec{u} \cdot \vec{m}_{(1)}^{(p)}}{D} \mathbf{I} \right) \right) \\ = 0, \end{aligned} \quad (\text{A26})$$

and the momentum balance for the mixture

$$\begin{aligned} \partial_t^{(1)} \rho \vec{u} + \partial_{\vec{x}} \cdot \left(\left(\hat{\tau} - \frac{1}{2} \right) c_s^2 \rho \left(\partial_{\vec{x}} \vec{u} + (\partial_{\vec{x}} \vec{u})^T - \frac{2}{D} (\partial_{\vec{x}} \cdot \vec{u}) \mathbf{I} \right) \right) \\ = 0, \end{aligned} \quad (\text{A27})$$

where the second-order moments of $\hat{f}_i^{1(p)}$ are obtained from Eq. (A6).

Summing Eqs. (A20)–(A27), we recover the balance equations, Eqs. (62)–(65).

- [1] X. Shan and H. Chen, Lattice Boltzmann model for simulating flows with multiple phases and components, *Phys. Rev. E* **47**, 1815 (1993).
- [2] S. Succi, *The Lattice Boltzmann Equation: For Fluid Dynamics and Beyond* (Oxford University Press, Oxford, 2001).
- [3] P. C. Philippi, K. K. Mattila, D. N. Siebert, L. O. E. dos Santos, L. A. Hegele Júnior, and R. Surmas, Lattice-Boltzmann equations for describing segregation in non-ideal mixtures, *J. Fluid Mech.* **713**, 564 (2012).
- [4] A. K. Gunstensen, D. H. Rothman, S. Zaleski, and G. Zanetti, Lattice Boltzmann model of immiscible fluids, *Phys. Rev. A* **43**, 4320 (1991).
- [5] A. K. Gunstensen and D. H. Rothman, Microscopic modeling of immiscible fluids in three dimensions by a lattice Boltzmann method, *Europhys. Lett.* **18**, 157 (1992).
- [6] X. Shan, Analysis and reduction of the spurious current in a class of multiphase lattice Boltzmann models, *Phys. Rev. E* **73**, 047701 (2006).
- [7] M. R. Swift, W. R. Osborn, and J. M. Yeomans, Lattice Boltzmann simulation of nonideal fluids, *Phys. Rev. Lett.* **75**, 830 (1995).
- [8] M. R. Swift, E. Orlandini, W. R. Osborn, and J. M. Yeomans, Lattice Boltzmann simulations of liquid-gas and binary fluid systems, *Phys. Rev. E* **54**, 5041 (1996).
- [9] X. He, S. Chen, and R. Zhang, A lattice boltzmann scheme for incompressible multiphase flow and its application in simulation of Rayleigh-Taylor instability, *J. Comput. Phys.* **152**, 642 (1999).
- [10] H. Liu, Q. Kang, C. R. Leonardi, S. Schmieschek, A. Narváez, B. D. Jones, J. R. Williams, A. J. Valocchi, and J. Harting, Multiphase lattice Boltzmann simulations for porous media applications, *Comp. Geosci.* **20**, 777 (2016).
- [11] H. Otomo, B. Crouse, M. Dressler, D. M. Freed, I. Staroselsky, R. Zhang, and H. Chen, Multi-component lattice Boltzmann models for accurate simulation of flows with wide viscosity variation, *Comput. Fluids* **172**, 674 (2018).
- [12] H. Huang, M. Krafczyk, and X. Lu, Forcing term in single-phase and Shan-Chen-type multiphase lattice Boltzmann models, *Phys. Rev. E* **84**, 046710 (2011).
- [13] Y. Peng, B. Wang, and Y. Mao, Study on force schemes in pseudopotential lattice Boltzmann model for two-phase flows, *Math. Probl. Eng.* **2018**, 9 (2018).
- [14] Q. Kang, D. Zhang, and S. Chen, Immiscible displacement in a channel: simulations of fingering in two dimensions, *Adv. Water Resour.* **27**, 13 (2004).
- [15] B. Dong, Y. Y. Yan, W. Li, and Y. Song, Lattice Boltzmann simulation of viscous fingering phenomenon of immiscible fluids displacement in a channel, *Comput. Fluids* **39**, 768 (2010).
- [16] M. L. Porter, E. T. Coon, Q. Kang, J. D. Moulton, and J. W. Carey, Multicomponent interparticle-potential lattice Boltzmann model for fluids with large viscosity ratios, *Phys. Rev. E* **86**, 036701 (2012).
- [17] J. Latt and B. Chopard, Lattice Boltzmann method with regularized pre-collision distribution functions, *Math. Comp. Simul.* **72**, 165 (2006).
- [18] R. Zhang, X. Shan, and H. Chen, Efficient kinetic method for fluid simulation beyond the Navier-Stokes equation, *Phys. Rev. E* **74**, 046703 (2006).
- [19] F. Gharibi and M. Ashrafizaadeh, Simulation of high-viscosity-ratio multicomponent fluid flow using a pseudopotential model based on the nonorthogonal central-moments lattice Boltzmann method, *Phys. Rev. E* **101**, 043311 (2020).
- [20] I. Ginzburg, Lattice Boltzmann modeling with discontinuous collision components: Hydrodynamic and advection-diffusion equations, *J. Stat. Phys.* **126**, 157 (2007).
- [21] H. Liu, L. Wu, Y. Ba, G. Xi, and Y. Zhang, A lattice Boltzmann method for axisymmetric multicomponent flows with high viscosity ratio, *J. Comput. Phys.* **327**, 873 (2016).
- [22] P. C. Philippi, L. O. Emerich Dos Santos, L. A. Hegele Jr, C. E. Pico Ortiz, D. N. Siebert, and R. Surmas, Thermodynamic consistency in deriving lattice Boltzmann models for describing segregation in nonideal mixtures, *Philos. Trans. R. Soc. A* **369**, 2292 (2011).
- [23] X. He, X. Shan, and G. D. Doolen, Discrete Boltzmann equation model for nonideal gases, *Phys. Rev. E* **57**, R13 (1998).
- [24] D. N. Siebert, P. C. Philippi, and K. K. Mattila, Consistent lattice Boltzmann equations for phase transitions, *Phys. Rev. E* **90**, 053310 (2014).
- [25] P. L. Bhatnagar, E. P. Gross, and M. Krook, A model for collision processes in gases. I. Small amplitude processes in charged and neutral one-component systems, *Phys. Rev.* **94**, 511 (1954).
- [26] P. C. Philippi, L. A. Hegele, L. O. E. dos Santos, and R. Surmas, From the continuous to the lattice Boltzmann equation: The discretization problem and thermal models, *Phys. Rev. E* **73**, 056702 (2006).
- [27] Y. Zhao, G. G. Pereira, S. Kuang, and B. Shi, On a modified pseudopotential lattice Boltzmann model for multicomponent flows, *Appl. Math. Lett.* **114**, 106926 (2021).
- [28] Z. Yu, L.-S. Fan *et al.*, Multirelaxation-time interaction-potential-based lattice Boltzmann model for two-phase flow, *Phys. Rev. E* **82**, 046708 (2010).
- [29] Q. Li, K. H. Luo, and X. J. Li, Forcing scheme in pseudopotential lattice Boltzmann model for multiphase flows, *Phys. Rev. E* **86**, 016709 (2012).
- [30] L.-S. Luo, Unified theory of lattice Boltzmann models for non-ideal gases, *Phys. Rev. Lett.* **81**, 1618 (1998).
- [31] X. Shan, X.-F. Yuan, and H. Chen, Kinetic theory representation of hydrodynamics: A way beyond the Navier–Stokes equation, *J. Fluid Mech.* **550**, 413 (2006).
- [32] Z. Guo, C. Zheng, and B. Shi, Discrete lattice effects on the forcing term in the lattice Boltzmann method, *Phys. Rev. E* **65**, 046308 (2002).
- [33] X. He, S. Chen, and G. D. Doolen, A novel thermal model for the lattice Boltzmann method in incompressible limit, *J. Comput. Phys.* **146**, 282 (1998).
- [34] P. Asinari, Multiple-relaxation-time lattice Boltzmann scheme for homogeneous mixture flows with external force, *Phys. Rev. E* **77**, 056706 (2008).
- [35] K. K. Mattila, L. A. Hegele, Jr., and P. C. Philippi, High-accuracy approximation of high-rank derivatives: Isotropic finite differences based on lattice-Boltzmann stencils, *Sci. World J.* **2014**, 1 (2014).
- [36] M. Sbragaglia, R. Benzi, L. Biferale, S. Succi, K. Sugiyama, and F. Toschi, Generalized lattice Boltzmann method with

- multirange pseudopotential, *Phys. Rev. E* **75**, 026702 (2007).
- [37] R. L. Bazarin, P. C. Philippi, A. Randles, and L. A. Hegele, Moments-based method for boundary conditions in the lattice Boltzmann framework: A comparative analysis for the lid driven cavity flow, *Comput. Fluids* **230**, 105142 (2021).
- [38] D. Halpern and D. Gaver III, Boundary element analysis of the time-dependent motion of a semi-infinite bubble in a channel, *J. Comput. Phys.* **115**, 366 (1994).
- [39] G. M. Kremer, *An Introduction to the Boltzmann Equation and Transport Processes in Gases* (Springer Science & Business Media, New York, 2010).